The nuclear oncogene SET controls DNA repair by KAP1 and HP1 retention to chromatin

Article (Published Version)

Article

Cell Reports

The Nuclear Oncogene SET Controls DNA Repair by KAP1 and HP1 Retention to Chromatin

Graphical Abstract

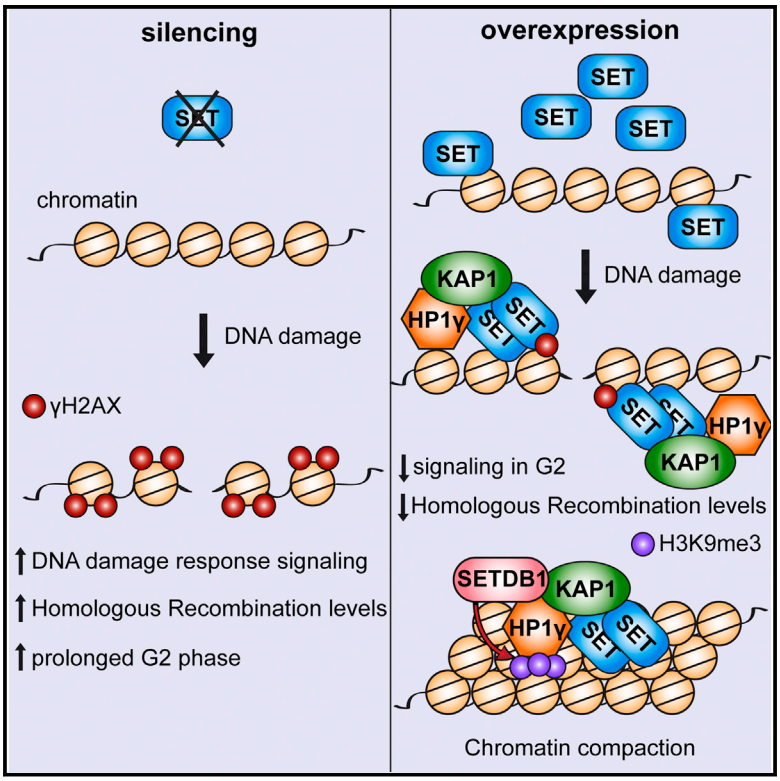

Highlights

- SET is recruited to DNA breaks to limit uncontrolled DDR and HR
- SET interacts with KAP1 and induces its retention on the chromatin
- SET overexpression induces chromatin compaction and inhibits repair by HR
- HP1γ inhibits DNA repair by limiting resection and HR factors' recruitment

Authors

Alkmini Kalousi,
Anne-Sophie Hoffbeck, ...,
Vassilis G. Gorgoulis, Evi Soutoglou

Correspondence

evisou@igbmc.fr

In Brief

Kalousi et al. show that SET is recruited to double-strand breaks to moderate the DNA damage response and inhibit resection and homologous recombination (HR) through increased retention of KAP1 and HP1γ on chromatin.

Kalousi et al., 2015, Cell Reports *11*, 149–163
April 07, 2015
http://dx.doi.org/10.1016/j.celrep.2015.03.005

CellPress

Cell Reports
Article

The Nuclear Oncogene SET Controls DNA Repair by KAP1 and HP1 Retention to Chromatin

Alkmini Kalousi,[1,8] Anne-Sophie Hoffbeck,[1,8] Platonas N. Selemenakis,[2] Jordan Pinder,[3,4] Kienan I. Savage,[5,9] Kum Kum Khanna,[5] Laurent Brino,[1] Graham Dellaire,[3,4] Vassilis G. Gorgoulis,[2,6,7] and Evi Soutoglou[1,*]

[1]Institut de Génétique et de Biologie Moléculaire et Cellulaire (IGBMC), UMR 7104 Centre National de la Recherche Scientifique (CNRS), UdS, INSERM U964, BP 10142, 67404 Illkirch Cedex, Strasbourg, France
[2]Molecular Carcinogenesis Group, Department of Histology and Embryology, School of Medicine, University of Athens, 11527 Athens, Greece
[3]Departments of Pathology and Biochemistry & Molecular Biology, Dalhousie University, B3H 4R2 Halifax, NS, Canada
[4]Beatrice Hunter Cancer Research Institute, B3H 4R2 Halifax, NS, Canada
[5]QIMR Berghofer Medical Research Institute, QLD 4006 Herston, Australia
[6]Faculty Institute of Cancer Sciences, University of Manchester, Manchester Academic Health Science Centre, M13 9PL Manchester, UK
[7]Biomedical Research Foundation, Academy of Athens, 11527 Athens, Greece
[8]Co-first author
[9]Present address: Centre for Cancer Research and Cell Biology, Queen's University Belfast, BT7 1NN Belfast, UK
*Correspondence: evisou@igbmc.fr
http://dx.doi.org/10.1016/j.celrep.2015.03.005

SUMMARY

Cells experience damage from exogenous and endogenous sources that endanger genome stability. Several cellular pathways have evolved to detect DNA damage and mediate its repair. Although many proteins have been implicated in these processes, only recent studies have revealed how they operate in the context of high-ordered chromatin structure. Here, we identify the nuclear oncogene SET (I2PP2A) as a modulator of DNA damage response (DDR) and repair in chromatin surrounding double-strand breaks (DSBs). We demonstrate that depletion of SET increases DDR and survival in the presence of radiomimetic drugs, while overexpression of SET impairs DDR and homologous recombination (HR)-mediated DNA repair. SET interacts with the Kruppel-associated box (KRAB)-associated co-repressor KAP1, and its overexpression results in the sustained retention of KAP1 and Heterochromatin protein 1 (HP1) on chromatin. Our results are consistent with a model in which SET-mediated chromatin compaction triggers an inhibition of DNA end resection and HR.

INTRODUCTION

Various types of agents from either exogenous or endogenous sources constantly assault DNA (Ciccia and Elledge, 2010; Hoeijmakers, 2001). DNA double-strand breaks (DSBs) are together with interstrand cross-links among the less frequent but the most toxic lesions because interaction between DNA ends from different DSBs can produce tumorigenic chromosome translocations (Misteli and Soutoglou, 2009). DSBs are repaired by two main pathways: non-homologous end-joining (NHEJ) and homologous recombination (HR) (Goodarzi and Jeggo, 2013). NHEJ is used by cells to join broken ends by simple re-ligation (Wang and Lees-Miller, 2013). HR takes advantage of the information encoded by the homologous template of the sister chromatid to repair the DSB in an error-free manner (Krejci et al., 2012).

DSBs trigger a complex cascade of signaling events known as the DNA damage response (DDR). During the DDR, DNA damage triggers the activation of phosphatidylinositol 3-kinases ATM/DNAPK/ATR (ataxia telangiectasia mutated/DNA-dependent protein kinase/ataxia telangiectasia and Rad3 related) and the activation of cell-cycle checkpoint kinases, which in turn pause the cell cycle until the DNA lesion is repaired (Bartek and Lukas, 2007).

DNA in the eukaryotic cell is complexed with histone proteins to form chromatin. Therefore, DNA repair generally occurs in the context of highly structured chromatin and, as a result, the cell has evolved mechanisms to open the chromatin structure and facilitate repair (Lemaître and Soutoglou, 2014; Soria et al., 2012). Emerging evidence suggests that the ability of repair factors to detect DNA lesions is determined by histone modifications around the lesion and involves chromatin-remodeling events (Polo and Jackson, 2011). The most prominent DNA-damage-induced histone modification in DNA DSB repair (DSBR) is the phosphorylation of the C-terminal tail of H2AX, referred to as γH2AX (Rogakou et al., 1998). Other chromatin proteins, such as the Kruppel-associated box (KRAB)-associated co-repressor KAP1, are also phosphorylated by ATM in response to DNA DSBs to further facilitate the decondensation of chromatin and allow efficient repair (Goodarzi et al., 2008; Ziv et al., 2006). Although there is increasing evidence that chromatin alterations are essential for efficient DSBR, the mechanisms underlying these chromatin changes are far from being fully understood.

In this study, we identified the oncoprotein SET as a modulator of the DDR using a small interfering RNA (siRNA)-based screen

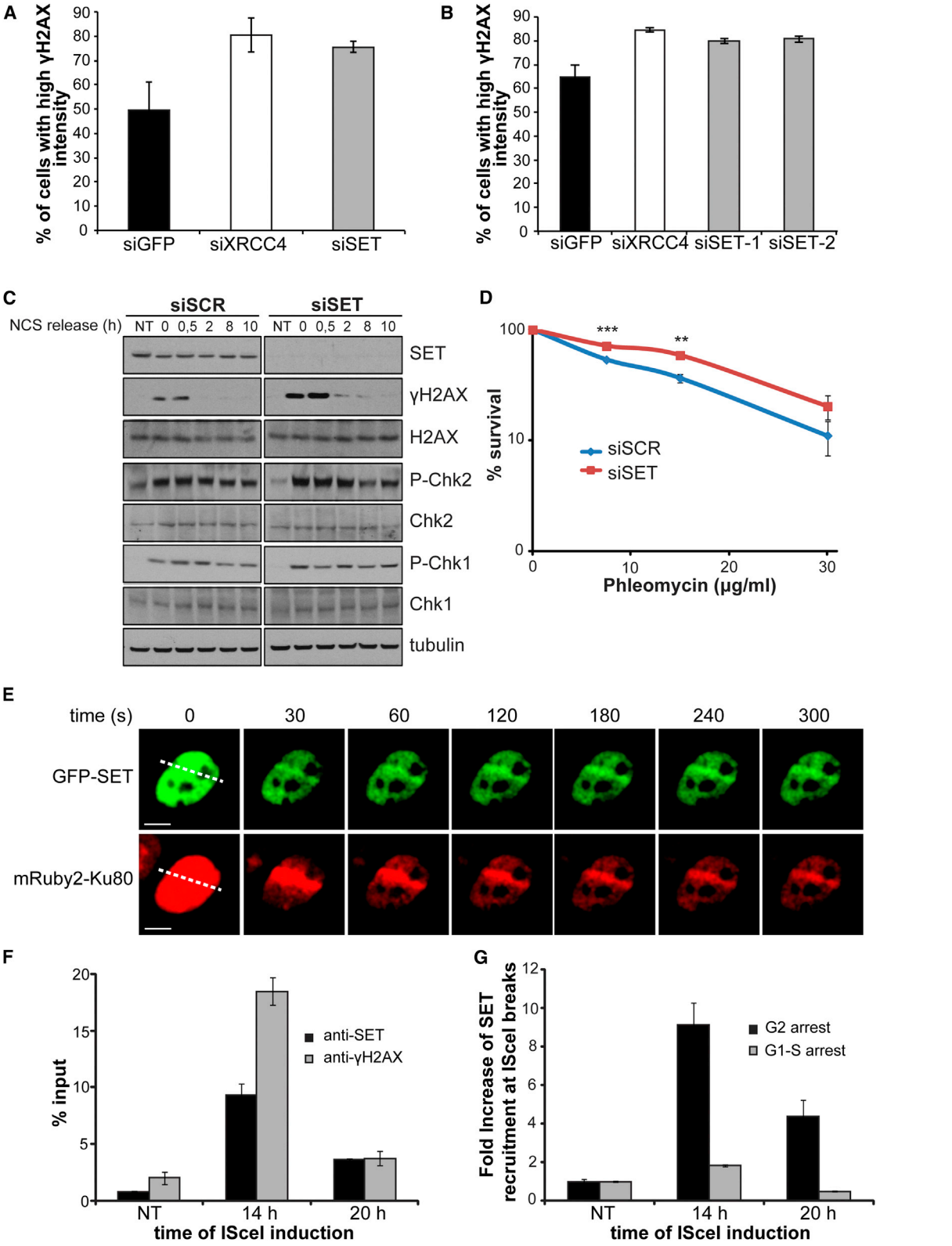

(legend on next page)

of chromatin-related proteins. We show that depletion of SET increases DDR and survival in the presence of radiomimetic drugs. On the other hand, SET overexpression impairs DDR, DNA break processing, and consequent repair by HR. SET interacts with the co-repressor KAP1, and its overexpression leads to the sustained retention of KAP1 and HP1 on chromatin. Our results suggest a model in which this retention triggers an inhibition of resection, impairing HR regulation.

RESULTS

The Nuclear Oncogene SET Is a Modulator of DDR in Chromatin Surrounding DSBs

To evaluate the impact of high-ordered chromatin structure in DDR and DNA repair in an unbiased way, we performed an siRNA screen using a library with chromatin-related proteins and their interaction partners. We identified the nuclear oncogene SET as a modulator of DDR since downregulation of SET resulted in a significant increase in levels of γH2AX foci remaining at 16 hr following Neocarzinostatin (NCS) treatment. This is similar to the DNA repair defect observed in cells depleted for XRCC4 (Figure 1A). Depletion of SET by two different siRNAs validated the phenotype observed in the primary screen (Figure 1B). The knockdown efficiency was monitored by qRT-PCR and western blot analysis (Figures S1A and S1B).

To validate the screen results in another cell type, we performed western blot analysis in control U2OS cells and in cells depleted for SET. We indeed observed higher damage-induced γH2AX levels in cells where SET was downregulated (Figure 1C). Interestingly, the level of γH2AX was increased immediately upon DNA damage and was sustained at a higher level until 8 hr later (Figure 1C). These results point to two different possibilities. First that depletion of SET results in persistent DNA damage, suggesting a role of SET in facilitating repair of DNA lesions. Another possible explanation is that downregulation of SET results in higher accessibility of H2AX to DDR kinases due to altered chromatin conformation, without affecting the number of unrepaired DNA breaks.

To differentiate between these two different possibilities, we used comet assays to measure the number of DNA lesions in control and SET-depleted cells. We did not observe a significant increase of breaks at any time upon DNA damage in cells lacking SET (Figure S1C). These results suggest that depletion of SET is affecting neither the initial number of DNA lesions nor their repair efficiency, as it was observed upon depletion of XRCC4, and point to the second possibility.

To further investigate the role of SET in checkpoint activation, we examined the phosphorylation status of Chk1 and Chk2 in controls cells and SET-depleted cells. Depletion of SET did not considerably alter Chk1 or Chk2 phosphorylation (Figure 1C), further strengthening the point that SET depletion does not lead to persistent DNA damage. Interestingly, and consistent with the enhanced DDR, SET-depleted cells exerted slower recovery from the G2/M checkpoint arrest from control cells (Figure S1D). To further evaluate the involvement of SET in genome integrity, we performed clonogenic survival assays in U2OS cells treated with the radiomimetic drug phleomycin. We observed that SET-depleted cells survive better in the presence of DNA damage than control cells (Figure 1D), suggesting that downregulation of SET renders DDR more efficient.

To investigate whether SET has a direct role in DDR, we tested the recruitment of SET fused to GFP in laser-induced breaks. Notably, SET was recruited to lesions instantly upon laser induction (Figure 1E). We also tested the recruitment of SET in endonuclease-induced breaks by chromatin immunoprecipitation (ChIP) (Lemaître et al., 2014). We found that SET is clearly recruited in I-SceI breaks, and we monitored the efficiency of break induction by γH2AX ChIP (Figures 1F and S1E). The observed fluctuations in SET recruitment in the laser microirradiation experiments prompted us to investigate whether the recruitment of SET is cell cycle specific. To this end, we performed ChIP experiments using SET antibody in cells arrested in G1/S or G2, and we observed that the recruitment of SET is more pronounced in cells arrested in G2 (Figures 1G and S1F).

All of the above results suggest that SET is recruited to DSBs to regulate DDR activation.

SET Overexpression Impedes DDR and Recruitment of HR Factors at Collapsed Forks and DSBs

The above findings support a potentially deleterious effect of high levels of SET. Indeed, SET is found to be highly overexpressed in a variety of cancers (Christensen et al., 2011; Li et al., 2012). To assess the impact of SET overexpression in genomic instability, we established a cellular model for SET overexpression in U2OS cells (Figures S2A–S2C). We generated U2OS stable cell lines overexpressing SET fused to GFP

Figure 1. The Nuclear Oncogene SET as a Factor Affecting the DDR

(A) SET as a major hit of a high-throughput siRNA screen to identify new chromatin-related DDR factors. HeLa cells were transfected with siGFP, siXRCC4, or siSET (pool) in 96-well plates. 72 hr post-transfection cells were treated with 50 ng/ml NCS for 15 min before being released for another 16 hr. Cells were then fixed and immunostained for γH2AX. Levels of γH2AX intensity were measured by an automated microscope.

(B) As in (A), the initial screen was validated using two individual siRNAs for SET (siSET-1 and -2).

(C) Western blot analysis of U2OS cells transfected with siSCR or siSET for 72 hr before being treated with 50 ng/ml NCS for 15 min and released for different time points is shown.

(D) Clonogenic survival of U2OS cells transfected with siSCR or siSET and treated with increasing concentrations of phleomycin. SEM represents the errors from three independent experiments. Statistical significance in all experiments was calculated using the t test (*$p < 0.05$, **$p < 0.01$, ***$p < 0.001$).

(E) Laser-induced DNA damage. Live cell imaging was performed after laser irradiation of U2OS cells co-expressing GFP-SET and mRuby2-Ku80 (scale bar represents 10 μm).

(F) ChIP for SET and γH2AX at the indicated time points upon Doxycycline addition in Hela111 cells is shown. Values were normalized to input DNA and are representative of two independent experiments.

(G) ChIP for SET at the indicated time points upon Doxycycline addition in Hela111 cells arrested in G1/S or G2 phase of the cell cycle. Values were normalized to the non-treated sample and are representative of two independent experiments.

(GFP-SET). A U2OS stable cell line overexpressing GFP was used as negative control. The level of overexpression of the SET protein was three to four times higher than the endogenous level of SET (Figure S2C). GFP-SET displayed nuclear localization similar to the endogenous protein (Figure S2B), and the overexpressed fusion protein did not alter the localization or the partition of endogenous SET to chromatin (Figure S2D).

To first test whether SET overexpression limits DDR, we evaluated γH2AX induction in GFP and GFP-SET cells upon NCS treatment. Interestingly, although, the DDR mounting in asynchronous SET-overexpressing cells was quite similar to control cells, γH2AX upon SET overexpression was significantly affected in cells arrested in G2 (Figure 2A). This observation is in line with the enhanced recruitment of SET in DNA lesions occurring in G2 (Figure 1G).

To assess the impact of SET overexpression in genomic instability, we performed clonogenic survival assays in U2OS GFP and GFP-SET cells in the presence of different damaging agents. We observed that cells overexpressing SET are mainly sensitive to the replication stress agent camptothecin and not phleomycin (Figures 2B and S2E). Therefore, our results strengthen the notion that SET overexpression affects the DDR or repair of lesions occurring in S-G2 phase.

In line with these results, cells overexpressing SET, although when not challenged do not demonstrate major changes in cell cycle or proliferation rates (Figures 2C and S2H), exerted slower progression through S-G2 phase compared to GFP cells when challenged with phleomycin (Figure S2F) and the replication stress agent hydroxyurea (HU) (Figure 2C), further suggesting an impairment in sensing or repairing lesions occurring during S phase. To further analyze this phenomenon with a specific S phase marker, we performed BrdU staining after treatment with HU in U2OS cells overexpressing GFP-SET or GFP (Figure S2G). In agreement with the previous observation, we observed a substantial increase in the proportion of challenged cells in S phase when SET was overexpressed (Figure 2C).

To investigate whether the delay in S and G2 phase progression is due to a defect in DDR at collapsed forks caused by SET overexpression, we compared γH2AX in control cells and in cells overexpressing SET, treated with HU and released 0, 8, 10, 12, 16, and 24 hr after the treatment. We found that, although the amount of collapsed forks in both conditions was the same, exemplified by the levels of RPA phosphorylation at S4/S8 (Figure 2D), there was a notable impairment in γH2AX induction (Figures 2D and S3A) in cells overexpressing SET. These results suggest an inhibitory role of SET in DDR signaling at stalled forks.

Next, we investigated whether SET overexpression had an impact on HR at collapsed forks. To this end, we assayed the recruitment of the HR repair factors BRCA1 and RAD51. Interestingly, the number of SET-overexpressing cells that displayed BRCA1 and RAD51 foci upon HU treatment was reduced at least to 50% compared to GFP-expressing cells (Figures 3A and 3B). Overall, these results show that overexpression of SET impedes DDR and recruitment of HR factors at collapsed forks.

To test whether a similar phenomenon was observed at endonuclease-induced DSBs in SET-overexpressing conditions, we used a cellular system in which a single DSB can be created at a specific genomic site (Lemaître et al., 2012; Soutoglou and Misteli, 2008). In this system, expression of I-SceI induces a DSB that can be visualized by monitoring localization of GFP-tagged lac repressor (GFP-lacI) and the early DDR marker γH2AX (Figures 3C and 3D). Remarkably, SET overexpression led to a defect in the recruitment of BRCA1 and RAD51 at the lacO/I-SceI array (Figure 3E). These observations were not due to chances of the cell-cycle profile, as SET overexpression had no impact on the cell cycle (Figure S3B). Similar results were obtained when RAD51 and BRCA1 foci were quantified in GFP and GFP-SET cells that were treated with NCS (Figures S3C–S3E).

We next used the lacO-lacI/I-SceI system to evaluate the impact of direct SET tethering to chromatin on the recruitment of HR proteins to DSBs. To this end, SET was fused to lacI and mCherry to generate mCherry-lacI-SET (Figures 4A and 4B). Stable association of SET on chromatin had a dramatic effect on BRCA1 and RAD51 loading at the breaks (Figure 4C). To test whether the defect in BRCA1 association with breaks in conditions that SET is overexpressed has an impact on resection of these breaks, we assessed recruitment of CtIP and phosphorylation of RPA upon tethering of SET at the lacO chromatin. Indeed, SET tethering affected the recruitment of CtIP and the phosphorylation of RPA at I-SceI breaks (Figure 4D). Similarly, SET tethering did not change the cell-cycle profile (Figure S4A).

To test whether the defect in resection and recruitment of HR factors when SET is overexpressed leads to a defect in HR, we used the DR-GFP system (Figure S4B; Pierce et al., 1999). As expected, depletion of BRCA1 led to a decrease in the HR efficiency (Figures 4E and S4C). In accordance with the previous observations of HR factor recruitment, SET overexpression decreased significantly the efficiency of HR without altering the cell-cycle patterns, and depletion of SET had the opposite effect (Figures 4E, S4C, and S4D).

Next we investigated whether the role of SET on HR had an impact on NHEJ. As depicted in Figure 4F, SET overexpression increased NHEJ levels. This result at the same time excluded the possibility of defective I-SceI cutting efficiency in the HR experiment due to increased chromatin compaction after SET overexpression. To study the role of SET in NHEJ, we checked the kinetics of recruitment of 53BP1 at the I-SceI breaks (Figures S4E–S4H). Interestingly, although the percentage of cells that exerted 53BP1 colocalization with the lacO/I-SceI locus was not different between control cells and cells overexpressing SET at a time point when there was peak DDR, inducible expression of I-SceI demonstrated that 53BP1 was recruited earlier in cells that overexpressed SET (Figures S4G and S4H).

SET Interacts with KAP1 and Facilitates KAP1 and HP1 Retention to Chromatin

To investigate the mechanism of action of SET, we searched for potential interaction partners. SET immunoprecipitation followed by mass spectrometry revealed co-repressor KAP1 (KRAB-associated protein-1) as an interacting partner of SET. To verify this interaction, we performed GFP-Trap immunoprecipitation experiments using the previously described U2OS GFP and GFP-SET cell lines. We observed an interaction between SET and KAP1 that did not depend on the presence of DNA damage (Figure 5A). Furthermore, the addition of Benzonase at the CoIP

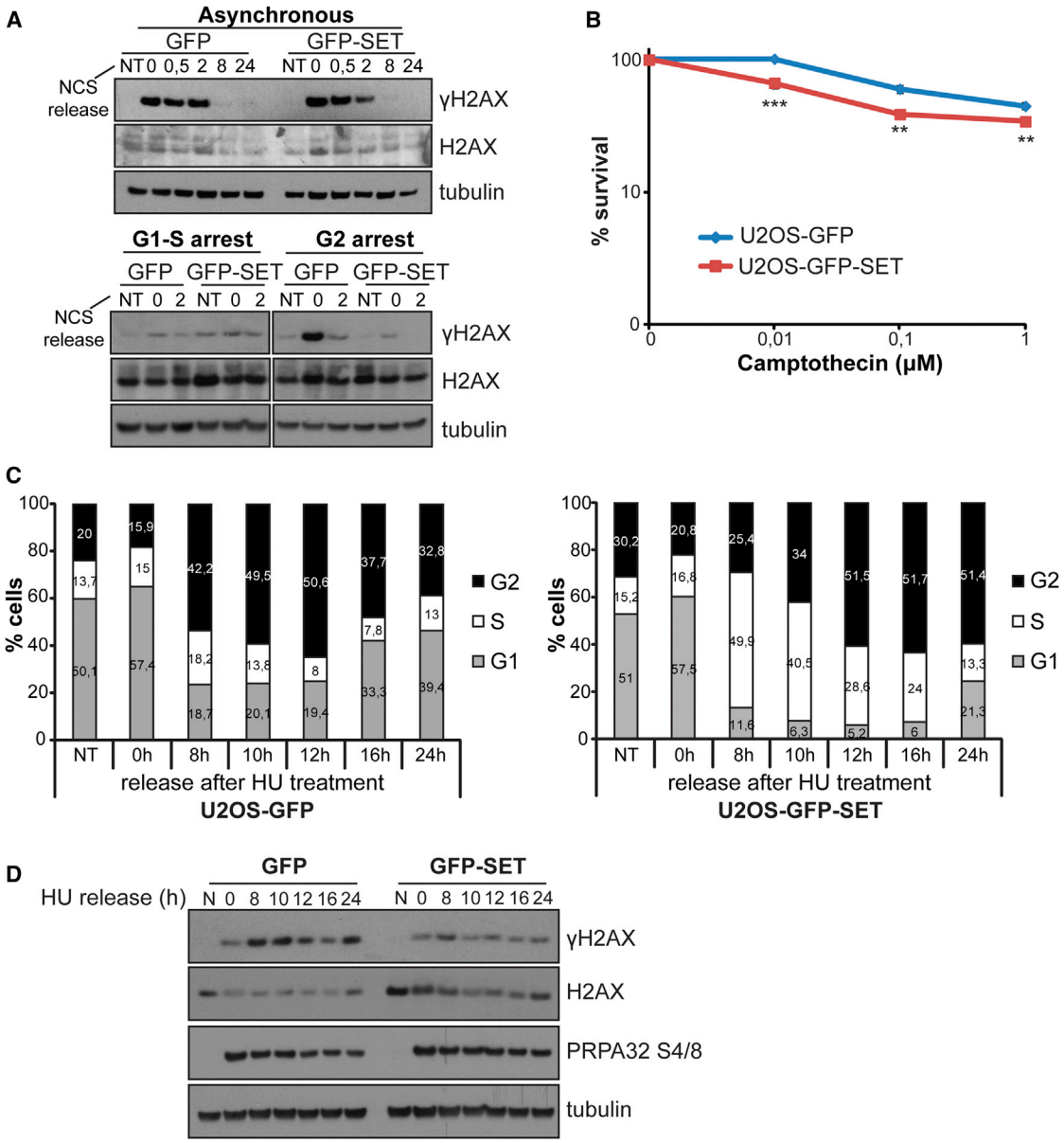

Figure 2. Overexpression of SET Affects Survival, Cell-Cycle Progression, and DDR Signaling during G2 and after Induction of Replication Stress

(A) Western blot analysis of asynchronous G1/S or G2-arrested U2OS GFP and U2OS GFP-SET cells treated with 50 ng/ml NCS for 15 min and released for the indicated time points is shown.

(B) Clonogenic survival of U2OS cells stably overexpressing GFP or GFP-SET with increasing concentrations of camptothecin. SEM represents the errors from three independent experiments.

(C) Cell-cycle analysis of U2OS GFP (left) and U2OS GFP-SET (right) cell lines after treatment with 10 mM HU for 24 hr (arrests cells in the border of G1-S) and release for the indicated time points is shown (analyzed using propidium iodide staining).

(D) Western blot analysis of U2OS GFP and U2OS GFP-SET cells treated with 10 mM HU for 24 hr and released for the indicated time points is shown.

demonstrated that the interaction of SET and KAP1 is DNA independent (Figure S5A).

To further explore the functional significance of SET and KAP1 interaction, and to test whether KAP1 is involved in any of the phenotypes related to SET overexpression, we examined its localization in cells overexpressing SET. Immunofluorescence staining showed similar KAP1 nuclear localization in U2OS cells overexpressing GFP-SET or GFP (Figure 5B). On the other hand, when immunofluorescence was performed under conditions in which all soluble proteins were pre-extracted before fixation, we observed a dramatic increase of KAP1 retention to chromatin when SET was overexpressed (Figure 5B, bottom, quantified in

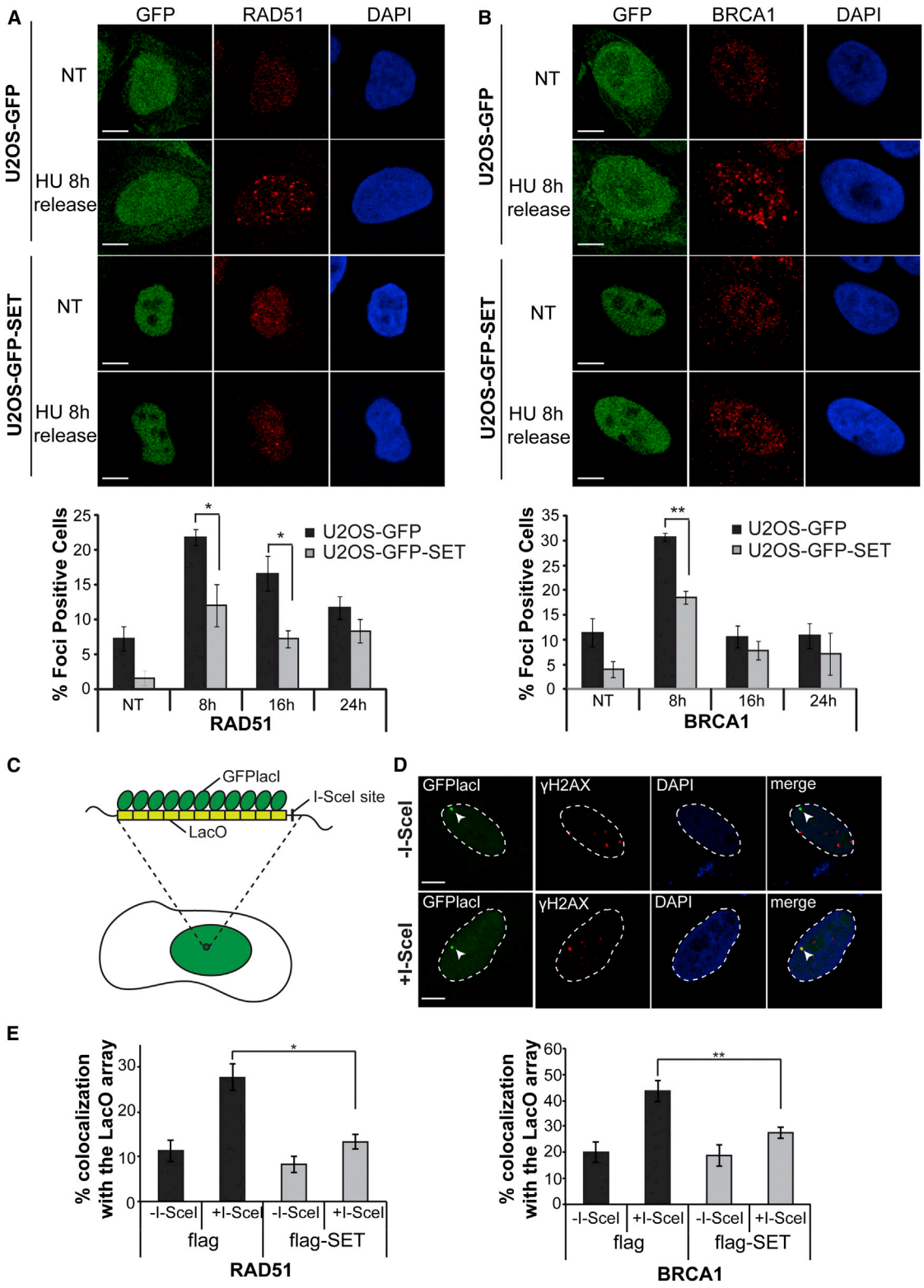

Figure 3. Overexpression of SET Impairs Recruitment of HR Factors on Collapsed Replication Forks and Endonuclease-Induced DSBs

(A and B) Immunofluorescence staining of U2OS GFP and GFP-SET cells with RAD51 and BRCA1 after treatment with 10 mM HU for 24 hr and release for another 8 hr (top) (scale bar represents 10 μm). Quantification is given of RAD51-foci-positive cells (>3 foci per cell) or BRCA1-foci-positive cells (>5 foci per cell) after

(legend continued on next page)

Figure 5C). The enhanced retention of KAP1 to chromatin in GFP-SET cells also was observed by biochemical cell fractionation (Figure 5D). To further strengthen this observation, we tested the chromatin retention of exogenously expressed cherry-KAP1 in GFP and GFP-SET cells after pre-extraction. We observed that, although the levels of cherry-KAP1 in GFP and GFP-SET cells were pretty similar (Figure S5B), the retention of cherry-KAP1 to chromatin after pre-extraction was enhanced in SET-overexpressing cells (Figures S5C and S5D). These results point to a role of SET in KAP1 chromatin retention.

KAP1 is known to mediate gene silencing by recruiting the methyltransferase SETDB1, which specifically tri-methylates histone H3 at Lys-9 (H3K9me3) (Schultz et al., 2001, 2002). To examine whether KAP1 chromatin retention in SET overexpression leads to increased H3 K9 methylation, we performed immunofluorescence in U2OS GFP and GFP-SET cells after pre-extraction of soluble proteins. Following the pattern of KAP1, H3K9me3 levels were also higher in SET-overexpressing conditions (Figure 5E, quantified in Figures 5F and S5E, right).

KAP1-mediated gene silencing also involves the recruitment of Heterochromatin protein 1 (HP1s: HP1α, β, and γ) through direct protein-protein interaction with KAP1, or through binding to H3K9me3 mark (Nielsen et al., 1999; Ryan et al., 1999). In line with the previous observations, SET overexpression led to a higher retention of HP1s in chromatin (Figure 5G). This phenomenon was particularly pronounced with HP1γ, which appeared globally perturbed, being more pan-nuclear than in the heterochromatic foci, and was not observed in another chromatin-bound protein like TBP (Figures 5G and S5F).

In line with the above observations, tethering of SET at the lacO led to the retention of KAP1 and HP1s at the locus (Figures 6A, 6B, S6A, and S6B). Among the HP1s, the most significant effect was observed with HP1γ (Figure 6B). Similar results were obtained when an I-SceI DSB was induced adjacent to the lacO locus. It is noteworthy that HP1γ colocalization with the array exerted a 40% reduction upon induction of the I-SceI break in cells expressing the lac repressor alone (Figure 6B), showing that HP1γ is evicted from the lacO chromatin upon DNA damage. Interestingly, upon SET tethering eviction of HP1γ was not observed, suggesting that SET inhibits the eviction of HP1γ and retains it stably bound to chromatin (Figure 6B).

Chromatin Compaction Inhibits Resection and Recruitment of HR Factors

Retention of HP1s in chromatin is likely to result in chromatin compaction. Indeed, cells overexpressing GFP-SET had smaller nuclear size compared to cells that expressed GFP (Figures S6C and S6D). Moreover, GFP-SET cells exerted resistance to micrococcal nuclease (Mnase) accessibility compared to GFP cells (Figure 6C), another indication of chromatin compaction. In agreement with this observation, detailed quantification of replication patterns in GFP and GFP-SET cells demonstrated that, although cells that overexpress SET have the same number of cells in S phase, they have a higher population of cells in late S phase than control cells, and SET-depleted cells have the reverse phenotype with less cells in late S (Figures S6E–S6H). These observations altogether point to a role of SET in chromatin compaction.

To investigate whether the chromatin compaction mediates the SET-dependent defect in loading of HR factors in DNA lesions, we alleviated chromatin compaction using Trichostatin A (TSA) (Tóth et al., 2004) and assessed RAD51 and BRCA1 foci formation at lacO/I-SceI breaks after SET tethering. As shown in Figure 6D, TSA treatment rescued the defect on BRCA1 and RAD51 at lacO/I-SceI breaks. Furthermore, TSA treatment rescued the recruitment of CtIP and RPA phosphorylation at the lacO/I-SceI locus, suggesting that chromatin compaction impacts resection (Figure 6E). Similarly, TSA treatment rescued the decrease observed in γH2AX at collapsed forks upon HU treatment (Figure 6F).

To test whether retention of KAP1 to chromatin is sufficient to induce the effects seen by SET tethering, we fused KAP1 to mCherry-lacI and tethered it to lacO. Interestingly, KAP1 tethering to lacO resulted in impairing the recruitment of RAD51, BRCA1, and CtIP after break induction with I-SceI (Figure S6I), which is in total accordance with the results coming from SET tethering on the chromatin. Moreover, tethering of KAP1 on the lacO array accumulated all three HP1s on the chromatin, but HP1γ seemed to be the one that was present almost 100% along with KAP1 (Figure S6J).

As HP1γ is the most pronounced at the lacO chromatin among all HP1s when SET is tethered, we investigated whether HP1γ retention could be part of the mechanism leading to the resection impairment observed in SET-overexpressing conditions. Therefore, we asked whether HP1γ tethering to the lacO array by fusion with lac repressor and with GFP could recapitulate the SET-tethering phenotype (Figures 7A and S7A–S7C). Tethering of HP1γ at the lacO array resulted in a substantial decrease in BRCA1, RAD51, CtIP, and phosphorylated RPA recruitment upon I-SceI break induction compared to the lac repressor alone (Figures 7A and 7B). This phenotype was specific to HP1γ since it was not observed upon tethering of HP1α or β (Figures 7A and 7B).

To further investigate the involvement of HP1γ in SET-dependent functions, we assayed resection and loading of BRCA1 and RAD51 at the lacO/I-SceI break upon SET tethering in control cells and cells depleted for HP1γ. Although when SET was tethered to chromatin CtIP, BRCA1, RAD51 loading, and

treatment with 10 mM HU and release for the indicated time points. Photos of at least 100 cells were analyzed for each condition. SEM represents the errors from three independent experiments.

(C) Schematic representation of the lacO-lacI/I-SceI system. An array of 256 repeats of the lacO sequence flanked by an I-SceI site is stably integrated into an U2OS cell line.

(D) Immunofluorescence of the GFP lacI-lacO U2OS cells with γH2AX in the presence or absence of I-SceI, indicating the colocalization of γH2AX foci with the lacO array in the presence of I-SceI (scale bar represents 10 μm), is shown.

(E) Quantification of the colocalization of RAD51, BRCA1, and P-RPA foci with the lacO array in at least 100 GFP lacI-lacO U2OS cells transfected with FLAG or FLAG-SET in the presence or absence of I-SceI. SEM represents the errors from three independent experiments.

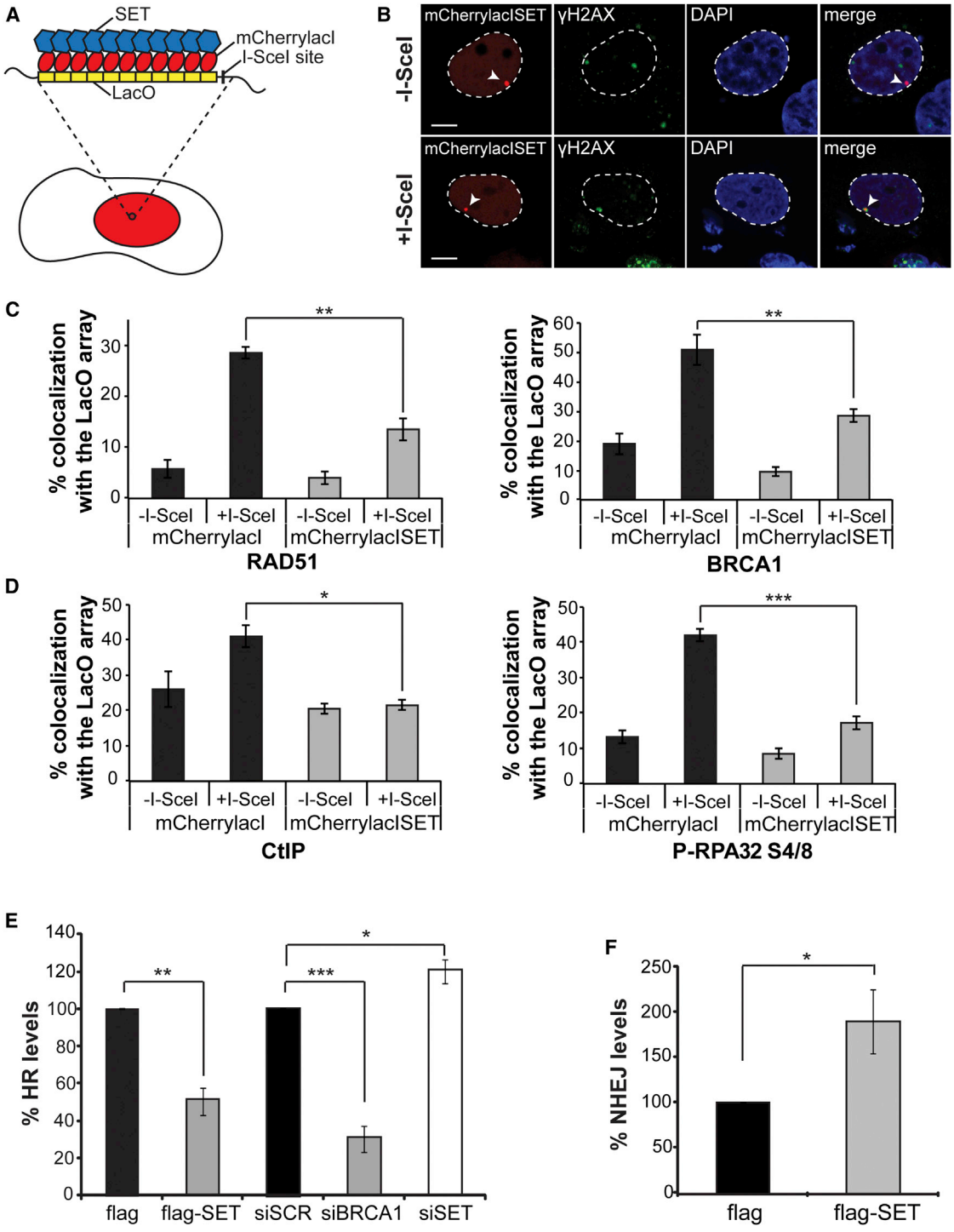

Figure 4. Tethering of SET on the Chromatin Impairs Resection and HR and Enhances NHEJ

(A) Schematic representation of SET tethering on the lacO-lacI/I-SceI system is shown.

(B) Immunofluorescence staining of the lacO U2OS cells transfected with mCherry-lacI-SET with γH2AX antibody in the presence or absence of I-SceI, indicating the colocalization of γH2AX foci with the lacO array in the presence of I-SceI (scale bar represents 10 μm), is shown.

(C and D) Quantification of the colocalization of RAD51, BRCA1, CtIP, and P-RPA32 S4/8 foci with the lacO array in at least 100 lacO U2OS cells transfected with mCherry-lacI or mCherry-lacI-SET in the presence or absence of I-SceI. SEM represents the errors from three independent experiments.

(legend continued on next page)

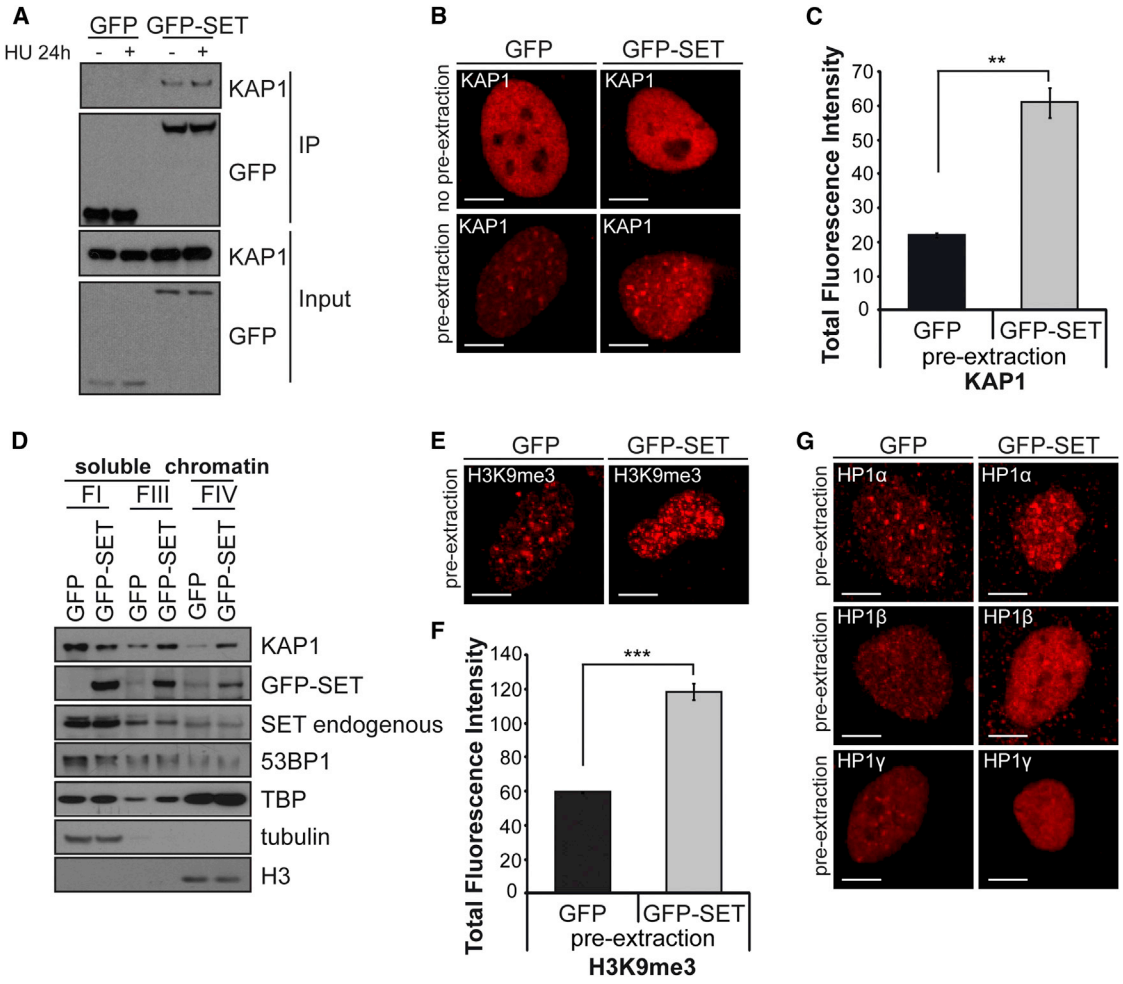

Figure 5. SET Interacts with KAP1 and Facilitates KAP1, SETDB1, and HP1 Retention on the Chromatin

(A) Immunoprecipitation (IP) of cell extracts from U2OS GFP and GFP-SET cells treated or not with 10 mM HU using the GFP-trap column. The inputs and eluates were analyzed by western blots against the proteins KAP1 and GFP.

(B) Immunofluorescence staining of U2OS GFP and GFP-SET cells with KAP1 antibody with or without pre-extraction is shown.

(C) Levels of KAP1 intensity after pre-extraction were measured by an automated microscope.

(D) Biochemical fractionation of U2OS GFP and U2OS GFP-SET cells. Fraction I (FI) represents the cytoplasmic fraction, Fraction III (FIII) the nuclear soluble fraction, and Fraction IV (FIV) the insoluble/chromatin fraction. All fractions were analyzed by western blot.

(E) Immunofluorescence staining of U2OS GFP and GFP-SET cells using antibodies against H3K9me3 after pre-extraction of nuclear soluble proteins prior to fixation is shown.

(F) Levels of H3K9me3 intensity after pre-extraction were measured by an automated microscope.

(G) Immunofluorescence staining of U2OS GFP and GFP-SET cells using antibodies against and HP1α, β, and γ after pre-extraction of nuclear soluble proteins prior to fixation is shown (scale bar represents 10 μm).

phosphorylated RPA at the lacO/I-SceI was decreased compared to cells that expressed mCherry-lacI alone, downregulation of HP1γ partially rescued this defect (Figures 7C and S7E). Downregulation of HP1α or β did not show any rescue and, on the contrary, affected resection and loading of HR proteins (Figure S7F), as shown previously (Baldeyron et al., 2011; Lee et al., 2013; Soria and Almouzni, 2013). The depletion of HP1s by siRNA was tested by western blot (Figure S7G). These findings point to a role of SET in KAP1 and HP1 retention to chromatin, and, when this is exaggerated, it results in impaired HR.

Depletion of SET in conditions where HP1γ was tethered to lacO chromatin did not rescue the recruitment of BRCA1 and

(E) FACS analysis of DR-GFP cells transfected with FLAG or FLAG-SET or siSCR, siSET, or siBRCA1 at the same time with either BFP- or BFP-I-SceI-expressing vector. SEM represents the errors from three independent experiments.

(F) FACS analysis of GCV6 cells transfected with FLAG or FLAG-SET at the same time with either BFP or BFP-I-SceI-expressing vector. SEM represents the errors from three independent experiments.

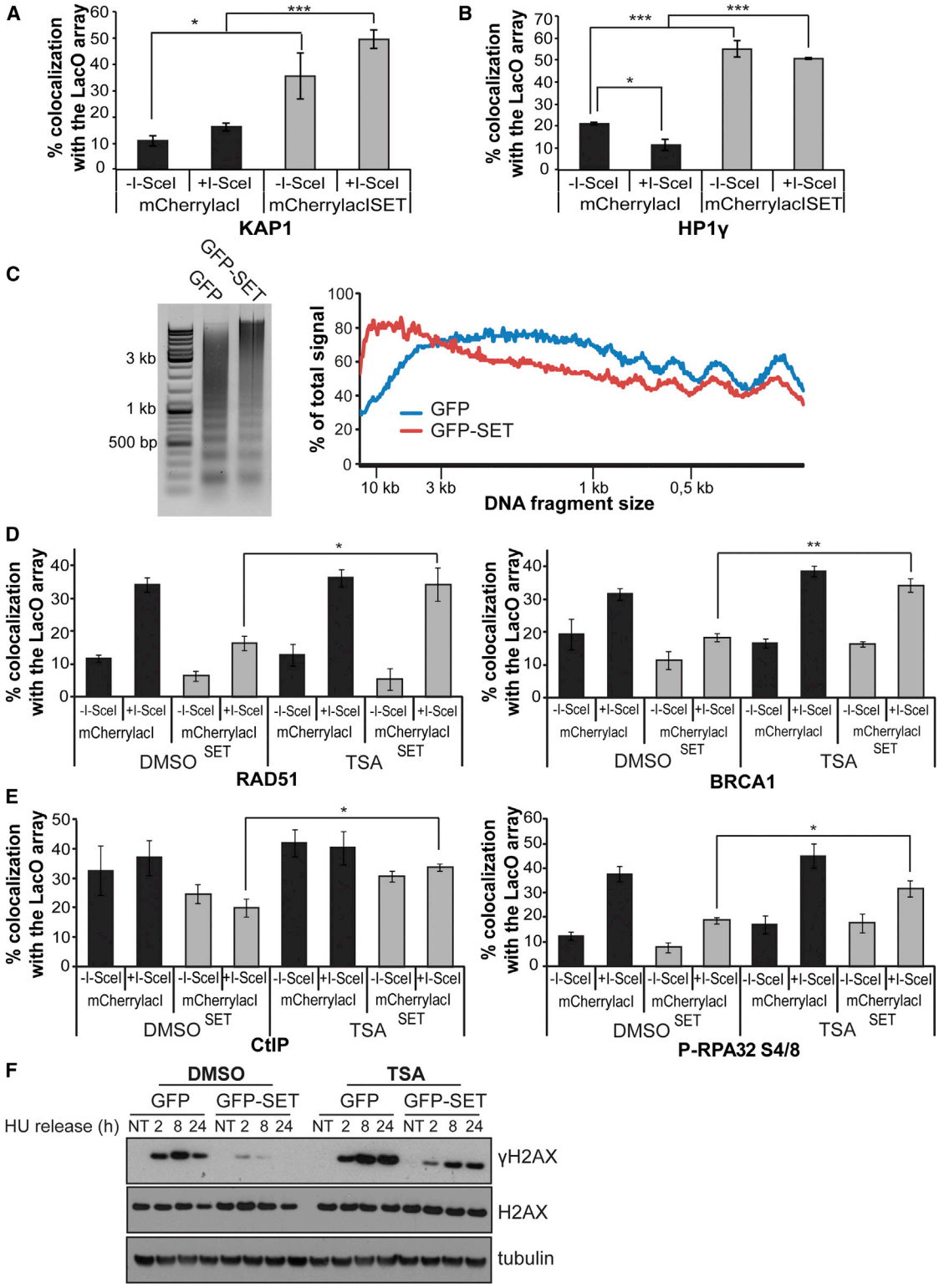

Figure 6. SET Tethering on Chromatin Induces Compaction through KAP1 and HP1γ Retention and TSA-Induced Relaxation Rescues Resection and HR Factors' Recruitment

(A and B) Quantification is given of the colocalization of KAP1 (A) and HP1γ (B) foci with the lacO array in at least 100 lacO U2OS cells transfected with mCherry-lacI or mCherry-lacI-SET in the presence or absence of I-SceI.

(legend continued on next page)

RAD51, suggesting that HP1γ is downstream of SET and, once tethered to chromatin by other means, can exert its function (Figure S7D).

Finally, the tight relationship among SET, H3K9me3, and HP1γ was examined by immunohistochemical and immunofluorescent means in serial sections from head and neck and colon cancers. SET had low expression in normal tissues, whereas its detection in cancerous lesions was evident (data not shown). Most importantly and in accordance with our model, the serial section analysis clearly depicted a correlation in increased levels of SET, H3K9me3, and HP1γ (Figures 7D and 7E).

Our results altogether propose a model in which SET associates with DNA breaks to moderate DDR and DNA repair by HR in the surrounding chromatin by regulating chromatin compaction. SET binds KAP1 and its overexpression leads to amplification of its normal function due to increased retention of KAP1 and HP1s to chromatin, leading to a repressive micro-enviroment for HR as the inefficient chromatin opening can inhibit resection and recruitment of major DNA repair factors (Figure 7F).

DISCUSSION

SET/TAF-Iβ, also known as I2PP2A and INHAT, was originally identified as a translocated gene in acute undifferentiated leukemia (Adachi et al., 1994). It is a multi-tasking protein and it was shown to be a potent inhibitor of phosphatase 2A (PP2A) (Li et al., 1996). It belongs to the NAP1 family of histone chaperones (Kawase et al., 1996; Muto et al., 2007). Other studies have shown that SET/TAF-Iβ binds to nucleosomal histones and inhibits histone acetylation by masking histone tails as a component of the INHAT complex (Kutney et al., 2004; Schneider et al., 2004). Here we describe a novel function of SET in DDR and DNA repair. We have found that SET is an endogenous modulator of DDR and, when depleted, enhances DDR and survival in radiomimetic drugs. In addition, we show that SET overexpression impairs DDR and HR and reduces survival in response to damaging agents. In line with our observations, SET depletion also was found to increase γH2AX in a high-content screen for chromatin-related proteins that affect DDR upon ionizing radiation (IR) (Floyd et al., 2013). The functions of SET in our study are independent from its role at the INHAT complex, since pp32, another component of the complex, did not exert similar functions in DDR and DNA repair as SET (data not shown).

In search of a potential mechanism of action of SET, we found that it interacts with KAP1 and mediates its retention to chromatin. Our results altogether suggest a model in which SET-dependent KAP1 chromatin retention leads to the retention of its interaction partner, the methyl-transferase SETDB1, and an increase in its target histone modification (Figures 5B–5F and S5E). Consequently, this heterochromatic mark triggers increased retention of the HP1 proteins to chromatin. In the presence of DNA damage, KAP1 and HP1s are not properly released from chromatin in SET-overexpressing cells, leading to inaccessibility of DNA repair factors and subsequent repair defect (Figure 4E). Given that the characterization of the interaction domain(s) of SET with KAP1 was not the focus of this study, future studies are necessary to uncover how SET recruits KAP1 and if its histone chaperone activity is connected with it.

Recent studies have highlighted the importance of KAP1 phosphorylation in HP1 and CHD3 release from heterochromatin to allow chromatin relaxation and access to DNA repair factors, leading to the efficient repair of heterochromatic lesions (Ayoub et al., 2008; Bolderson et al., 2012; Garvin et al., 2013; Goodarzi et al., 2011; White et al., 2012). For HP1β, this release was dependent on its phosphorylation by casein kinase II (Ayoub et al., 2008). On the other hand, all three HP1 isoforms are shown to accumulate in DNA lesions through their chromoshadow domain (Luijsterburg et al., 2009; Soria and Almouzni, 2013). These contradictory findings can be reconciled to a model in which HP1 mobilization from DSBs is followed by its accumulation at these or other sites of damage. In accordance with this bimodal behavior of HP1s, although ATM is activated to induce chromatin relaxation by KAP1 phosphorylation immediately after damage, it was shown that, in breaks in which resection had occurred, ATM activity was diminished, pointing to a need for chromatin reconstitution for late steps of HR to occur (Geuting et al., 2013). Our results are in agreement with the necessity of open chromatin for DDR and DNA end resection.

Our results reveal distinct behavior of HP1 isoforms in response to DNA damage. First, we show that exclusively HP1γ, and not α or β, is released from I-SceI-induced breaks. Moreover, persistent binding of HP1γ to chromatin inhibits resection and subsequent strand invasion, exemplified by the defective recruitment of RAD51 and BRCA1 (Figures 7A and 7B). Our observations are in line with recent data that revealed differences in how the HP1 isoforms regulate HR (Soria and Almouzni, 2013). Although, HP1α and HP1β promote RPA phosphorylation, recruitment of RAD51, and HR stimulation, HP1γ plays an inhibitory role, suggesting that its release is necessary for efficient repair by HR. Also, the effect of chromatin compaction on DNA end resection observed by SET overexpression is in keeping with recent studies, which found that HR is activated at DSBs located within actively transcribed genes that reside in euchromatin (Aymard et al., 2014; Jha and Strahl, 2014; Pai et al., 2014).

One study described SET as a chaperone of histone H1 and demonstrated that SET is regulating the eviction of histone H1 from chromatin (Kato et al., 2011). Moreover, knockout of some of the histone H1 isoforms leads to an increase in DDR due to chromatin decondensation (Murga et al., 2007). Our data show that SET overexpression leads to chromatin compaction and reduced DDR that fits more with enhanced binding of H1 to chromatin than enhanced eviction. Possible explanations for this discrepancy are that prolonged overexpression of SET leads

(C) MNase digestion of chromatin from U2OS GFP and GFP-SET nuclei and quantification (right) are shown.
(D and E) As in (A) and (B), the lacO U2OS cells also were treated with either DMSO or TSA for 8 hr prior to fixation and cells were immunostained against RAD51, BRCA1, CtIP, and P-RPA32 S4/8. SEM represents the errors from three independent experiments.
(F) Western blot analysis of whole-cell extracts of U2OS GFP and GFP-SET cells that were treated with 10 mM HU for 24 hr and released in DMSO or TSA for the indicated time points is shown.

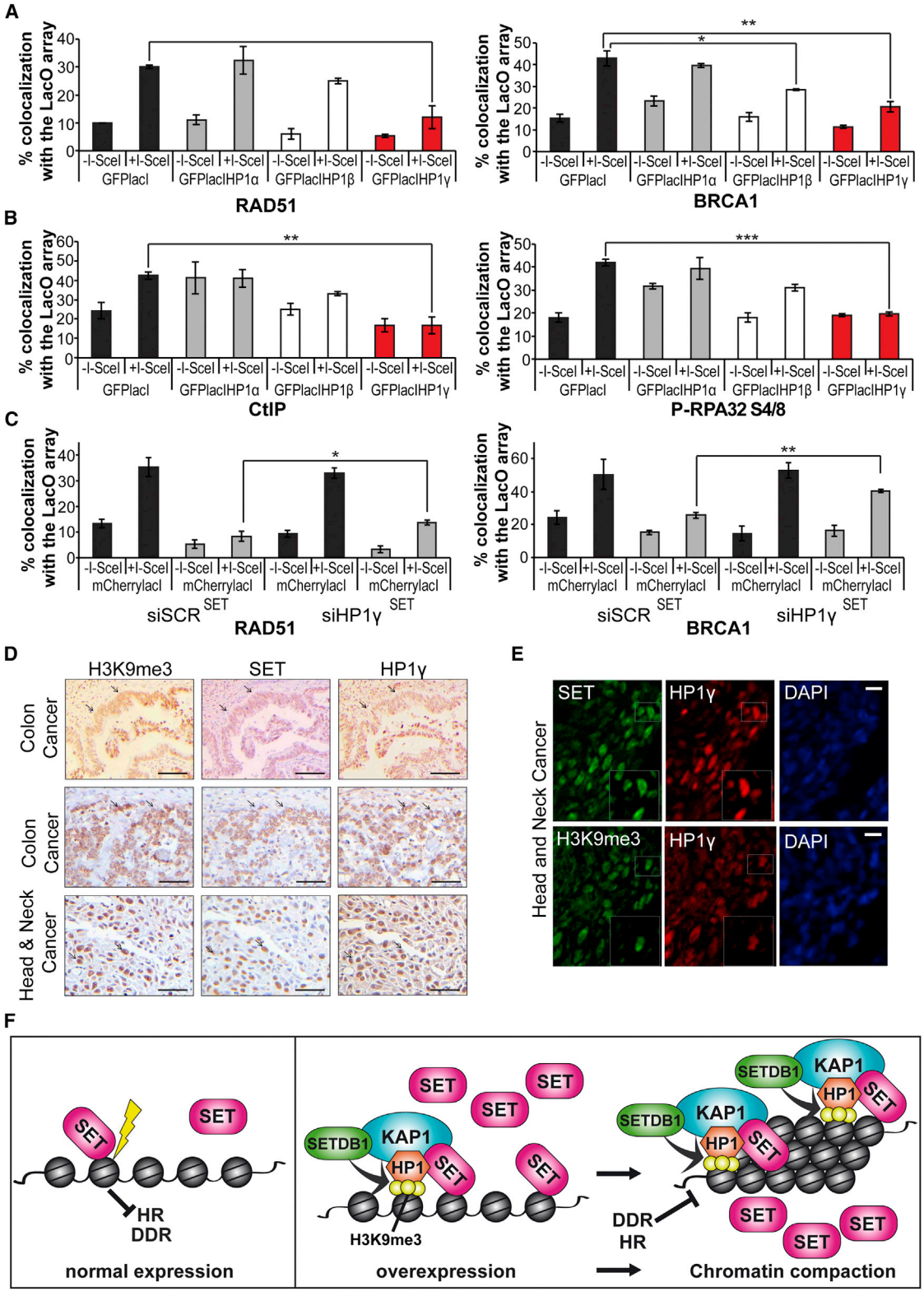

(legend on next page)

to an imbalance of the different histone H1 isoforms, leading to complex phenotypes, or that the functions of SET on DSB repair are independent of its histone chaperone activity.

SET is highly overexpressed in various types of cancers (Adachi et al., 1994; Christensen et al., 2011; Jiang et al., 2011; Leopoldino et al., 2012; Li et al., 2012; Ouellet et al., 2006), and in certain cases SET levels correlate with disease severity (Christensen et al., 2011). Although, it was proposed that SET leads to tumorigenesis because it inhibits the tumor suppressor PP2A or metastasis suppressor NM23-H1 (Switzer et al., 2011), our results suggest that defective DNA repair by HR in cells that overexpress SET also might contribute to the initiation of carcinogenesis and/or progression.

Moreover, SET has been shown to interact with the tumor suppressor p53 (Kim et al., 2012). SET inhibits p53 acetylation thus repressing transcription of its target genes, leading to impairment of p53-dependent cell-cycle arrest and apoptosis. These results are fitting with the observation that SET is overexpressed in cancer. Although, we haven't directly tested the activation of p53 target genes in our system, the reduced cell survival upon DNA damage in SET-overexpressing cells could be attributed to impaired apoptosis and cell-cycle arrest.

Therefore, SET represents an attractive therapeutic target for cancer therapy. In keeping with this, recent studies have reported the development of peptides like COG112 (Switzer et al., 2011) that inhibit the binding of SET with PP2A or NM23-H1 and release them from the SET inhibitory effect. In addition, our results demonstrating that SET-overexpressing cells are hypersensitive to replication stress agents, such as camptothecin (Figure 2B), suggest that these types of agents, which are widely used in the clinic, may be exploited to target tumors expressing high levels of SET.

EXPERIMENTAL PROCEDURES

Cell Culture and Transfections

U2OS and U2OS-lacO-ISceI-Tet19 cells were cultured at 37°C in DMEM supplemented with glucose (4.5 g/l), 10% fetal calf serum, and gentamycine (40 μg/ml). U2OS GFP and U2OS GFP-SET cells were cultured as U2OS cells with the addition of 0.8 g/ml G418. FuGene 6 (Promega) and Interferin (Polyplus Transfection) were used for transient transfections of plasmids and siRNA transfections (20 nM final concentration of siRNA), respectively.

Laser Microirradiation

For 405-nm UV-laser irradiation, experiments were carried out as described by Kruhlak et al. (2006).

ChIP

The ChIP was performed as previously (Lemaître et al., 2014) with a few changes as described in the Supplemental Experimental Procedures.

GFP-Trap

U2OS GFP and GFP-SET cells were collected in lysis buffer (10 mM Tris/Cl [pH 7.5], 150 mM NaCl, 0.5 mM EDTA, 0.5% NP40, and protease inhibitor cocktail [Roche]), incubated for 20 min on ice and centrifuged for another 20 min (14,000 rpm, 4°C). The supernatant was incubated with GFP-trap beads (Chromotek) for 2 hr at 4°C under rotation. Beads were washed and eluted in SDS sample buffer.

Biochemical Fractionation

Biochemical fractionation was carried out as previously described (Andegeko et al., 2001).

HR and NHEJ Assay

DR-GFP cells (HR) and GCV6 cells (NHEJ) (Rass et al., 2009) were transfected with pcDNA-FLAG or pcDNA-FLAG-SET or the appropriate siRNAs in combination with either BFP-C1 or BFP-C1-I-SceI. Then 72 hrs after transfection, the cells were collected and fixed with 4% paraformaldehyde in PBS for 10 min at room temperature. Samples were submitted to fluorescence-activated cell sorting (FACS) analyzed by FlowJo.

MNase Assay

The assay was carried out as previously described with a few changes (Ziv et al., 2006). In brief, cells were harvested and nuclei immediately isolated using hypotonic buffer. Freshly isolated nuclei were digested for 30 s at 25°C with MNase (Roche) at a concentration of 10 U per 75 μl digestion buffer (15 mM Tris-HCl [pH 7.4], 60 mM KCl, 15 mM NaCl, 0.25 M sucrose, 1 mM $CaCl_2$, and 0.5 mM DTT). Genomic DNA was purified and separated by electrophoresis in 1.2% agarose gel.

SUPPLEMENTAL INFORMATION

Supplemental Information includes Supplemental Experimental Procedures and seven figures and can be found with this article online at http://dx.doi.org/10.1016/j.celrep.2015.03.005.

AUTHOR CONTRIBUTIONS

A.K. and A.-S.H. designed and performed experiments. P.N.S., J.P., and K.I.S. performed experiments. K.K.K., L.B., G.D., and V.G.G. supervised experiments. E.S. conceived the study and designed experiments. A.K. and E.S. wrote the paper.

ACKNOWLEDGMENTS

We thank Thomais Papamarcaki (University of Ioannina) for the GFP-SET plasmid. A.K. was supported by the Fondation ARC; A.-S.H. was supported by Allocation Presidence fellowhip and Fondation pour la Recherche Médicale (FRM); and research in the E.S. laboratory is funded by the Human Frontiers

Figure 7. HP1γ Tethering on Chromatin Inhibits Resection and Recruitment of HR Factors, Whereas HP1γ Silencing Partially Rescues Repair from SET-Induced Compaction

(A and B) Quantification is given of the colocalization of RAD51, BRCA1, CtIP, and P-RPA32 S4/8 foci with the lacO array in at least 100 lacO U2OS cells transfected with GFP lacI or GFP lacIHP1α, GFP lacIHP1β, or GFP lacIHP1γ in the presence or absence of I-SceI.

(C) Quantification is given of the colocalization of RAD51 and BRCA1 foci with the lacO array in at least 100 lacO U2OS cells transfected with siSCR or siHP1γ, followed by transfection with mCherry-lacI or mCherry-lacI-SET in the presence or absence of I-SceI. SEM represents the errors from three independent experiments.

(D) Colocalization of SET, H3K9me3, and HP1γ in colon and head and neck carcinomas. Immunohistochemical staining of SET, H3K9me3, and HP1γ in serial sections indicating their colocalization in the nucleus of cancer cells (arrows) is shown (scale bars represent 100 μm [top] and 50 μm [middle and bottom]).

(E) Double immunofluoresence of SET-HP1γ and HP1γ-H3K9me3 in serial sections of head and neck carcinomas indicating their concomitant overexpression is shown (scale bar represents 10 μm).

(F) Schematic representation of the proposed model is given.

Science program (HFSP CDA), the Agence Nationale de la Recherché (program Blanc), the Centre National de la Recherche Scientifique (CNRS, ATIP), the Institut National du Cancer (INCA libre) and the European FP7 framework (Marie Curie Reintegration grant), the Fondation Schlumberger (FSER), and the EMBO Young Investigator Program (EMBO YIP). V.G.G. is financially supported by the Greek GSRT program of Excellence II (Aristeia II). Work in the G.D. laboratory was supported by a Discover Grant from the Natural Science and Engineering Research Council (NSERC), and J.P. was supported by a Postdoctoral trainee award from the Beatrice Hunter Cancer Research Institute (BHCRI) with funds provided by Harvey Graham Cancer Research Fund as part of The Terry Fox Strategic Health Research Training Program in Cancer Research at CIHR. K.K.K. acknowledges the National Health and Medical Research Council (NHMRC) Senior Principal Research Fellowships (ID 613638) and NHMRC Program grant (ID 1017028).

Received: September 12, 2014
Revised: January 15, 2015
Accepted: February 27, 2015
Published: March 26, 2015

REFERENCES

Adachi, Y., Pavlakis, G.N., and Copeland, T.D. (1994). Identification and characterization of SET, a nuclear phosphoprotein encoded by the translocation break point in acute undifferentiated leukemia. J. Biol. Chem. *269*, 2258–2262.

Andegeko, Y., Moyal, L., Mittelman, L., Tsarfaty, I., Shiloh, Y., and Rotman, G. (2001). Nuclear retention of ATM at sites of DNA double strand breaks. J. Biol. Chem. *276*, 38224–38230.

Aymard, F., Bugler, B., Schmidt, C.K., Guillou, E., Caron, P., Briois, S., Iacovoni, J.S., Daburon, V., Miller, K.M., Jackson, S.P., and Legube, G. (2014). Transcriptionally active chromatin recruits homologous recombination at DNA double-strand breaks. Nat. Struct. Mol. Biol. *21*, 366–374.

Ayoub, N., Jeyasekharan, A.D., Bernal, J.A., and Venkitaraman, A.R. (2008). HP1-beta mobilization promotes chromatin changes that initiate the DNA damage response. Nature *453*, 682–686.

Baldeyron, C., Soria, G., Roche, D., Cook, A.J., and Almouzni, G. (2011). HP1alpha recruitment to DNA damage by p150CAF-1 promotes homologous recombination repair. J. Cell Biol. *193*, 81–95.

Bartek, J., and Lukas, J. (2007). DNA damage checkpoints: from initiation to recovery or adaptation. Curr. Opin. Cell Biol. *19*, 238–245.

Bolderson, E., Savage, K.I., Mahen, R., Pisupati, V., Graham, M.E., Richard, D.J., Robinson, P.J., Venkitaraman, A.R., and Khanna, K.K. (2012). Kruppel-associated Box (KRAB)-associated co-repressor (KAP-1) Ser-473 phosphorylation regulates heterochromatin protein 1β (HP1-β) mobilization and DNA repair in heterochromatin. J. Biol. Chem. *287*, 28122–28131.

Christensen, D.J., Chen, Y., Oddo, J., Matta, K.M., Neil, J., Davis, E.D., Volkheimer, A.D., Lanasa, M.C., Friedman, D.R., Goodman, B.K., et al. (2011). SET oncoprotein overexpression in B-cell chronic lymphocytic leukemia and non-Hodgkin lymphoma: a predictor of aggressive disease and a new treatment target. Blood *118*, 4150–4158.

Ciccia, A., and Elledge, S.J. (2010). The DNA damage response: making it safe to play with knives. Mol. Cell *40*, 179–204.

Floyd, S.R., Pacold, M.E., Huang, Q., Clarke, S.M., Lam, F.C., Cannell, I.G., Bryson, B.D., Rameseder, J., Lee, M.J., Blake, E.J., et al. (2013). The bromodomain protein Brd4 insulates chromatin from DNA damage signalling. Nature *498*, 246–250.

Garvin, A.J., Densham, R.M., Blair-Reid, S.A., Pratt, K.M., Stone, H.R., Weekes, D., Lawrence, K.J., and Morris, J.R. (2013). The deSUMOylase SENP7 promotes chromatin relaxation for homologous recombination DNA repair. EMBO Rep. *14*, 975–983.

Geuting, V., Reul, C., and Löbrich, M. (2013). ATM release at resected double-strand breaks provides heterochromatin reconstitution to facilitate homologous recombination. PLoS Genet. *9*, e1003667.

Goodarzi, A.A., and Jeggo, P.A. (2013). The repair and signaling responses to DNA double-strand breaks. Adv. Genet. *82*, 1–45.

Goodarzi, A.A., Noon, A.T., Deckbar, D., Ziv, Y., Shiloh, Y., Löbrich, M., and Jeggo, P.A. (2008). ATM signaling facilitates repair of DNA double-strand breaks associated with heterochromatin. Mol. Cell *31*, 167–177.

Goodarzi, A.A., Kurka, T., and Jeggo, P.A. (2011). KAP-1 phosphorylation regulates CHD3 nucleosome remodeling during the DNA double-strand break response. Nat. Struct. Mol. Biol. *18*, 831–839.

Hoeijmakers, J.H. (2001). Genome maintenance mechanisms for preventing cancer. Nature *411*, 366–374.

Jha, D.K., and Strahl, B.D. (2014). An RNA polymerase II-coupled function for histone H3K36 methylation in checkpoint activation and DSB repair. Nat. Commun. *5*, 3965.

Jiang, Q., Zhang, C., Zhu, J., Chen, Q., and Chen, Y. (2011). The set gene is a potential oncogene in human colorectal adenocarcinoma and oral squamous cell carcinoma. Mol. Med. Rep. *4*, 993–999.

Kato, K., Okuwaki, M., and Nagata, K. (2011). Role of Template Activating Factor-I as a chaperone in linker histone dynamics. J. Cell Sci. *124*, 3254–3265.

Kawase, H., Okuwaki, M., Miyaji, M., Ohba, R., Handa, H., Ishimi, Y., Fujii-Nakata, T., Kikuchi, A., and Nagata, K. (1996). NAP-I is a functional homologue of TAF-I that is required for replication and transcription of the adenovirus genome in a chromatin-like structure. Genes Cells *1*, 1045–1056.

Kim, J.Y., Lee, K.S., Seol, J.E., Yu, K., Chakravarti, D., and Seo, S.B. (2012). Inhibition of p53 acetylation by INHAT subunit SET/TAF-Iβ represses p53 activity. Nucleic Acids Res. *40*, 75–87.

Krejci, L., Altmannova, V., Spirek, M., and Zhao, X. (2012). Homologous recombination and its regulation. Nucleic Acids Res. *40*, 5795–5818.

Kruhlak, M.J., Celeste, A., Dellaire, G., Fernandez-Capetillo, O., Müller, W.G., McNally, J.G., Bazett-Jones, D.P., and Nussenzweig, A. (2006). Changes in chromatin structure and mobility in living cells at sites of DNA double-strand breaks. J. Cell Biol. *172*, 823–834.

Kutney, S.N., Hong, R., Macfarlan, T., and Chakravarti, D. (2004). A signaling role of histone-binding proteins and INHAT subunits pp32 and Set/TAF-Ibeta in integrating chromatin hypoacetylation and transcriptional repression. J. Biol. Chem. *279*, 30850–30855.

Lee, Y.H., Kuo, C.Y., Stark, J.M., Shih, H.M., and Ann, D.K. (2013). HP1 promotes tumor suppressor BRCA1 functions during the DNA damage response. Nucleic Acids Res. *41*, 5784–5798.

Lemaître, C., and Soutoglou, E. (2014). Double strand break (DSB) repair in heterochromatin and heterochromatin proteins in DSB repair. DNA Repair (Amst.) *19*, 163–168.

Lemaître, C., Fischer, B., Kalousi, A., Hoffbeck, A.S., Guirouilh-Barbat, J., Shahar, O.D., Genet, D., Goldberg, M., Betrand, P., Lopez, B., et al. (2012). The nucleoporin 153, a novel factor in double-strand break repair and DNA damage response. Oncogene *31*, 4803–4809.

Lemaître, C., Grabarz, A., Tsouroula, K., Andronov, L., Furst, A., Pankotai, T., Heyer, V., Rogier, M., Attwood, K.M., Kessler, P., et al. (2014). Nuclear position dictates DNA repair pathway choice. Genes Dev. *28*, 2450–2463.

Leopoldino, A.M., Squarize, C.H., Garcia, C.B., Almeida, L.O., Pestana, C.R., Sobral, L.M., Uyemura, S.A., Tajara, E.H., Silvio Gutkind, J., and Curti, C. (2012). SET protein accumulates in HNSCC and contributes to cell survival: antioxidant defense, Akt phosphorylation and AVOs acidification. Oral Oncol. *48*, 1106–1113.

Li, M., Makkinje, A., and Damuni, Z. (1996). The myeloid leukemia-associated protein SET is a potent inhibitor of protein phosphatase 2A. J. Biol. Chem. *271*, 11059–11062.

Li, C., Ruan, H.Q., Liu, Y.S., Xu, M.J., Dai, J., Sheng, Q.H., Tan, Y.X., Yao, Z.Z., Wang, H.Y., Wu, J.R., and Zeng, R. (2012). Quantitative proteomics reveal up-regulated protein expression of the SET complex associated with hepatocellular carcinoma. J. Proteome Res. *11*, 871–885.

Luijsterburg, M.S., Dinant, C., Lans, H., Stap, J., Wiernasz, E., Lagerwerf, S., Warmerdam, D.O., Lindh, M., Brink, M.C., Dobrucki, J.W., et al. (2009).

Heterochromatin protein 1 is recruited to various types of DNA damage. J. Cell Biol. *185*, 577–586.

Misteli, T., and Soutoglou, E. (2009). The emerging role of nuclear architecture in DNA repair and genome maintenance. Nat. Rev. Mol. Cell Biol. *10*, 243–254.

Murga, M., Jaco, I., Fan, Y., Soria, R., Martinez-Pastor, B., Cuadrado, M., Yang, S.M., Blasco, M.A., Skoultchi, A.I., and Fernandez-Capetillo, O. (2007). Global chromatin compaction limits the strength of the DNA damage response. J. Cell Biol. *178*, 1101–1108.

Muto, S., Senda, M., Akai, Y., Sato, L., Suzuki, T., Nagai, R., Senda, T., and Horikoshi, M. (2007). Relationship between the structure of SET/TAF-Ibeta/INHAT and its histone chaperone activity. Proc. Natl. Acad. Sci. USA *104*, 4285–4290.

Nielsen, A.L., Ortiz, J.A., You, J., Oulad-Abdelghani, M., Khechumian, R., Gansmuller, A., Chambon, P., and Losson, R. (1999). Interaction with members of the heterochromatin protein 1 (HP1) family and histone deacetylation are differentially involved in transcriptional silencing by members of the TIF1 family. EMBO J. *18*, 6385–6395.

Ouellet, V., Le Page, C., Guyot, M.C., Lussier, C., Tonin, P.N., Provencher, D.M., and Mes-Masson, A.M. (2006). SET complex in serous epithelial ovarian cancer. Int. J. Cancer *119*, 2119–2126.

Pai, C.C., Deegan, R.S., Subramanian, L., Gal, C., Sarkar, S., Blaikley, E.J., Walker, C., Hulme, L., Bernhard, E., Codlin, S., et al. (2014). A histone H3K36 chromatin switch coordinates DNA double-strand break repair pathway choice. Nat. Commun. *5*, 4091.

Pierce, A.J., Johnson, R.D., Thompson, L.H., and Jasin, M. (1999). XRCC3 promotes homology-directed repair of DNA damage in mammalian cells. Genes Dev. *13*, 2633–2638.

Polo, S.E., and Jackson, S.P. (2011). Dynamics of DNA damage response proteins at DNA breaks: a focus on protein modifications. Genes Dev. *25*, 409–433.

Rass, E., Grabarz, A., Plo, I., Gautier, J., Bertrand, P., and Lopez, B.S. (2009). Role of Mre11 in chromosomal nonhomologous end joining in mammalian cells. Nat. Struct. Mol. Biol. *16*, 819–824.

Rogakou, E.P., Pilch, D.R., Orr, A.H., Ivanova, V.S., and Bonner, W.M. (1998). DNA double-stranded breaks induce histone H2AX phosphorylation on serine 139. J. Biol. Chem. *273*, 5858–5868.

Ryan, R.F., Schultz, D.C., Ayyanathan, K., Singh, P.B., Friedman, J.R., Fredericks, W.J., and Rauscher, F.J., 3rd. (1999). KAP-1 corepressor protein interacts and colocalizes with heterochromatic and euchromatic HP1 proteins: a potential role for Krüppel-associated box-zinc finger proteins in heterochromatin-mediated gene silencing. Mol. Cell. Biol. *19*, 4366–4378.

Schneider, R., Bannister, A.J., Weise, C., and Kouzarides, T. (2004). Direct binding of INHAT to H3 tails disrupted by modifications. J. Biol. Chem. *279*, 23859–23862.

Schultz, D.C., Friedman, J.R., and Rauscher, F.J., 3rd. (2001). Targeting histone deacetylase complexes via KRAB-zinc finger proteins: the PHD and bromodomains of KAP-1 form a cooperative unit that recruits a novel isoform of the Mi-2alpha subunit of NuRD. Genes Dev. *15*, 428–443.

Schultz, D.C., Ayyanathan, K., Negorev, D., Maul, G.G., and Rauscher, F.J., 3rd. (2002). SETDB1: a novel KAP-1-associated histone H3, lysine 9-specific methyltransferase that contributes to HP1-mediated silencing of euchromatic genes by KRAB zinc-finger proteins. Genes Dev. *16*, 919–932.

Soria, G., and Almouzni, G. (2013). Differential contribution of HP1 proteins to DNA end resection and homology-directed repair. Cell Cycle *12*, 422–429.

Soria, G., Polo, S.E., and Almouzni, G. (2012). Prime, repair, restore: the active role of chromatin in the DNA damage response. Mol. Cell *46*, 722–734.

Soutoglou, E., and Misteli, T. (2008). Activation of the cellular DNA damage response in the absence of DNA lesions. Science *320*, 1507–1510.

Switzer, C.H., Cheng, R.Y., Vitek, T.M., Christensen, D.J., Wink, D.A., and Vitek, M.P. (2011). Targeting SET/I(2)PP2A oncoprotein functions as a multi-pathway strategy for cancer therapy. Oncogene *30*, 2504–2513.

Tóth, K.F., Knoch, T.A., Wachsmuth, M., Frank-Stöhr, M., Stöhr, M., Bacher, C.P., Müller, G., and Rippe, K. (2004). Trichostatin A-induced histone acetylation causes decondensation of interphase chromatin. J. Cell Sci. *117*, 4277–4287.

Wang, C., and Lees-Miller, S.P. (2013). Detection and repair of ionizing radiation-induced DNA double strand breaks: new developments in nonhomologous end joining. Int. J. Radiat. Oncol. Biol. Phys. *86*, 440–449.

White, D., Rafalska-Metcalf, I.U., Ivanov, A.V., Corsinotti, A., Peng, H., Lee, S.C., Trono, D., Janicki, S.M., and Rauscher, F.J., 3rd. (2012). The ATM substrate KAP1 controls DNA repair in heterochromatin: regulation by HP1 proteins and serine 473/824 phosphorylation. Mol. Cancer Res. *10*, 401–414.

Ziv, Y., Bielopolski, D., Galanty, Y., Lukas, C., Taya, Y., Schultz, D.C., Lukas, J., Bekker-Jensen, S., Bartek, J., and Shiloh, Y. (2006). Chromatin relaxation in response to DNA double-strand breaks is modulated by a novel ATM- and KAP-1 dependent pathway. Nat. Cell Biol. *8*, 870–876.

Cell Reports

Supplemental Information

The Nuclear Oncogene SET Controls DNA Repair by KAP1 and HP1 Retention to Chromatin

Alkmini Kalousi, Anne-Sophie Hoffbeck, Platonas N. Selemenakis, Jordan Pinder, Kienan I. Savage, Kum Kum Khanna, Laurent Brino, Graham Dellaire, Vassilis G. Gorgoulis, and Evi Soutoglou

Figure S1 (Related to Figure 1)

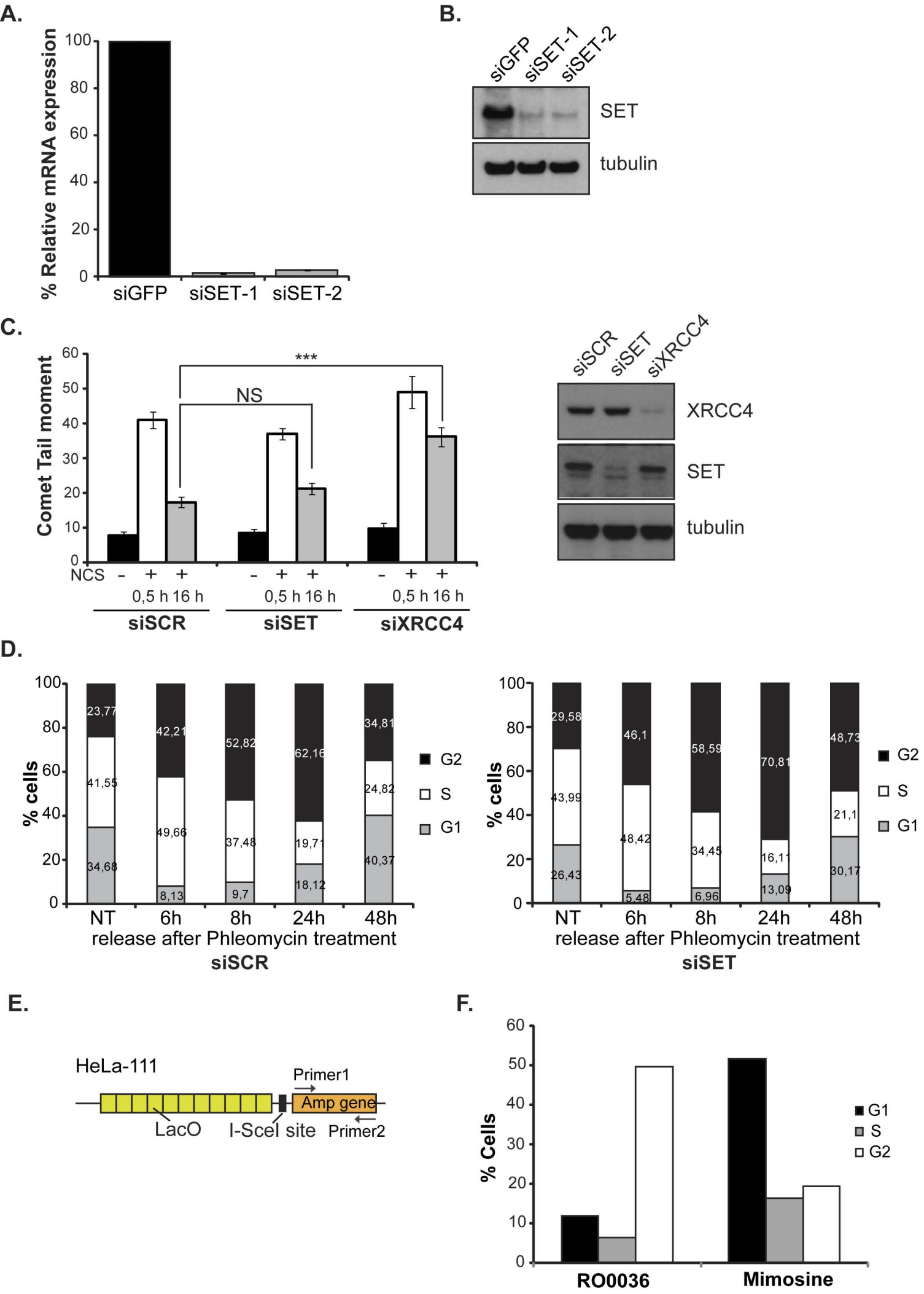

Figure S2 (Related to Figure 2)

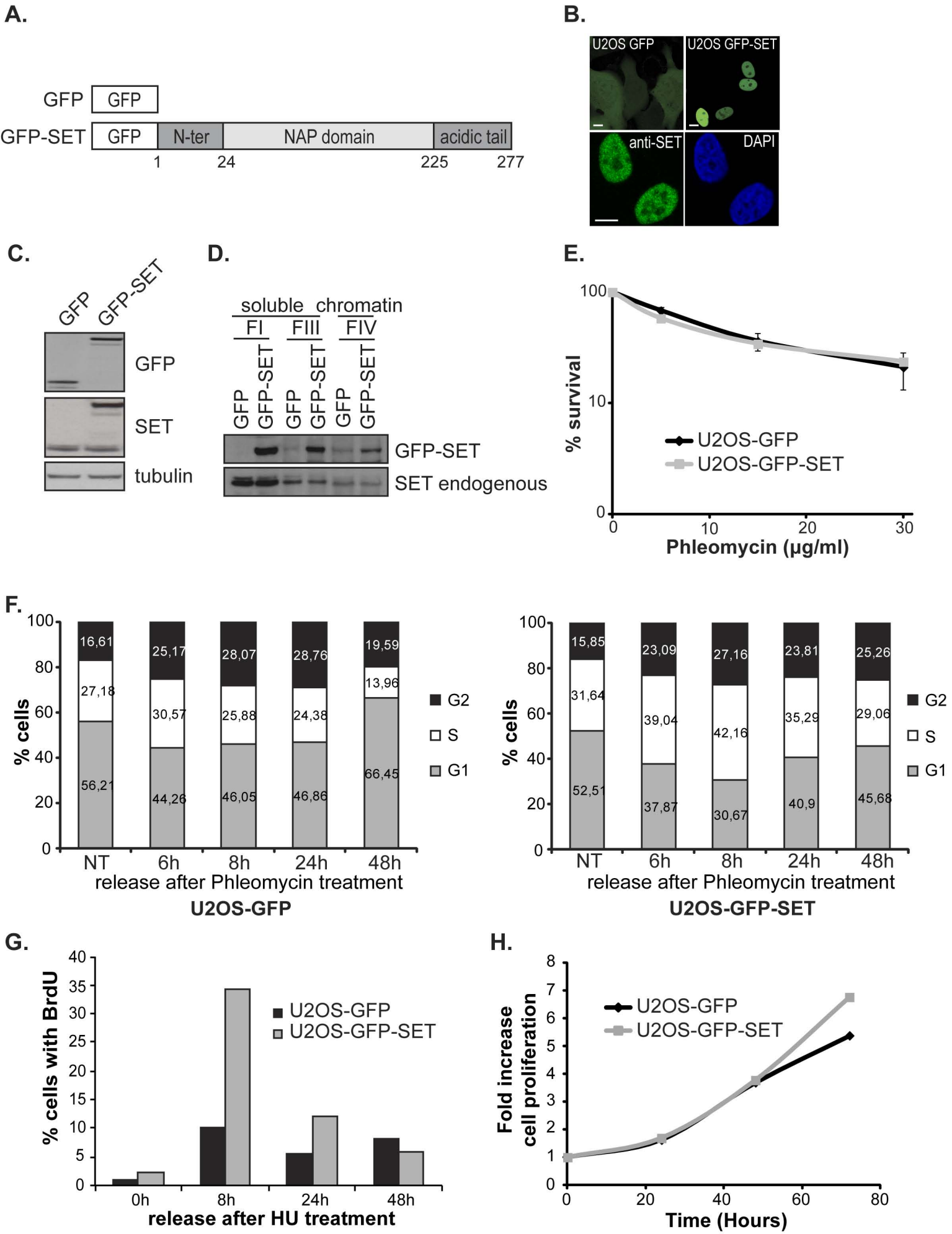

Figure S3 (Related to Figure 3)

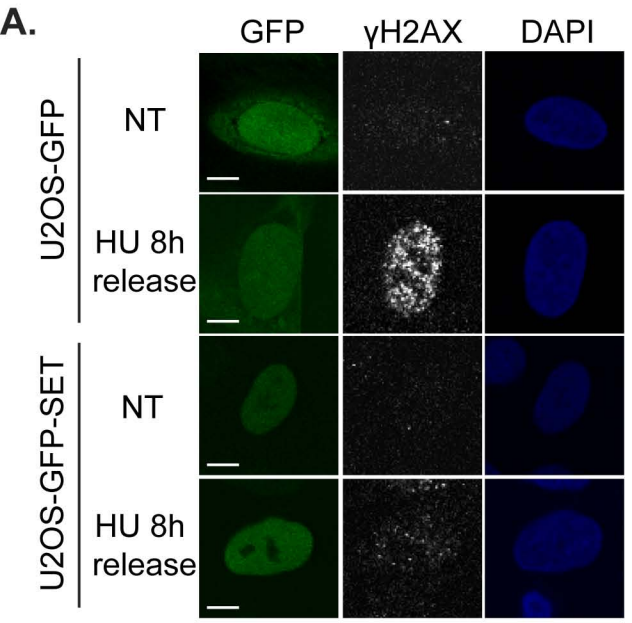

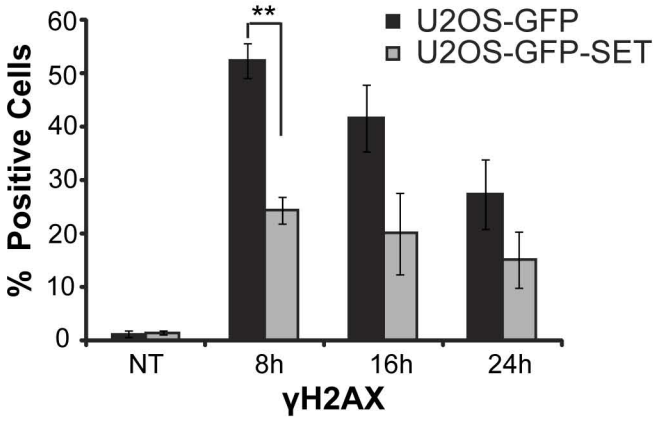

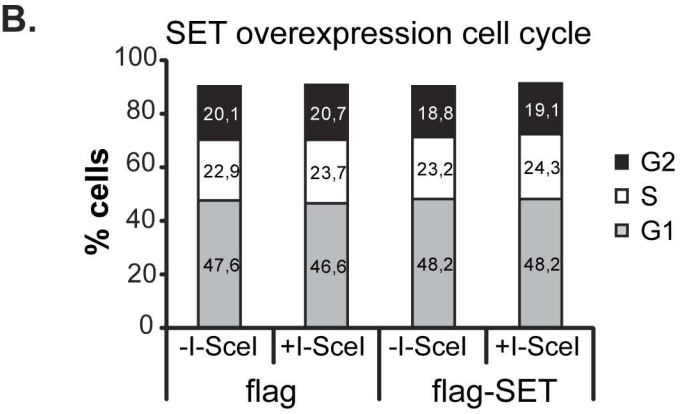

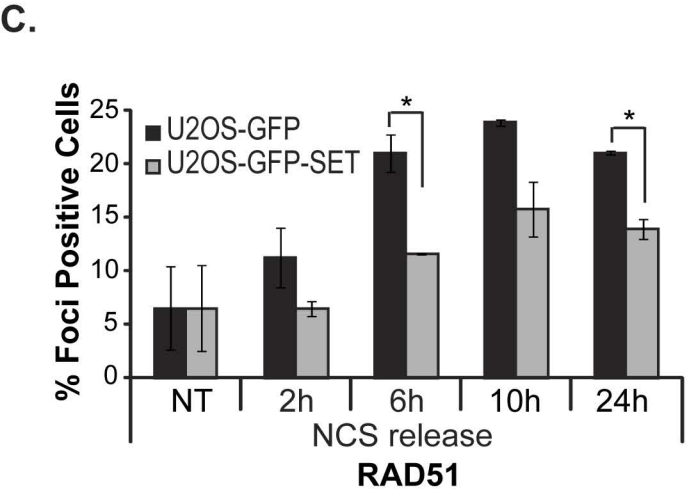

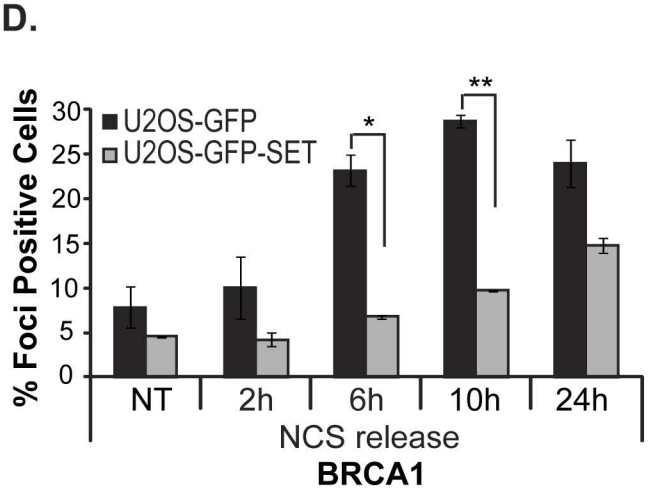

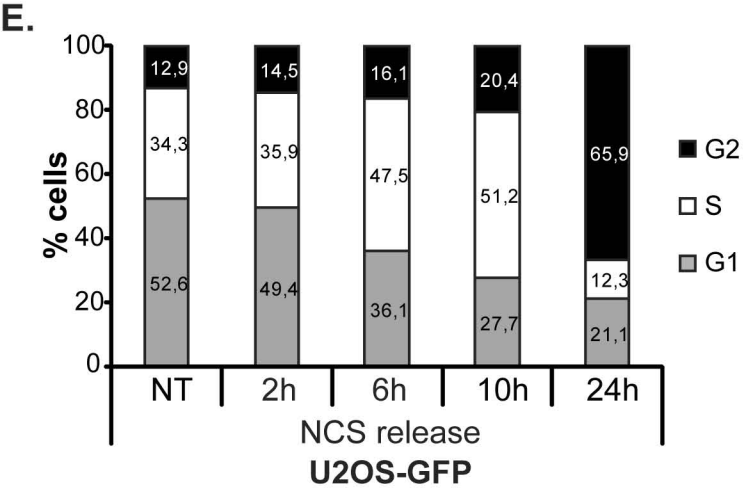

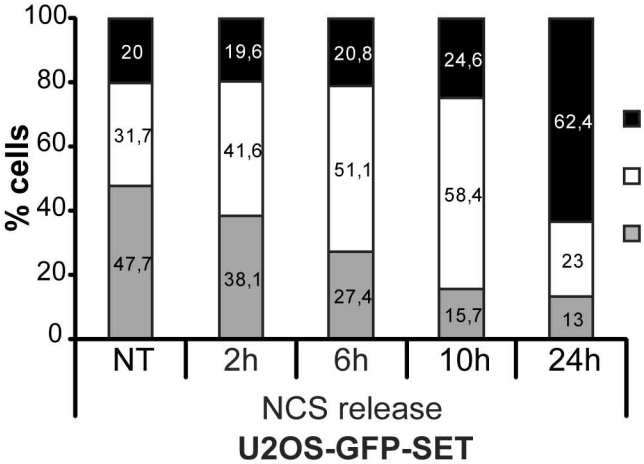

Figure S4 (Related to Figure 4)

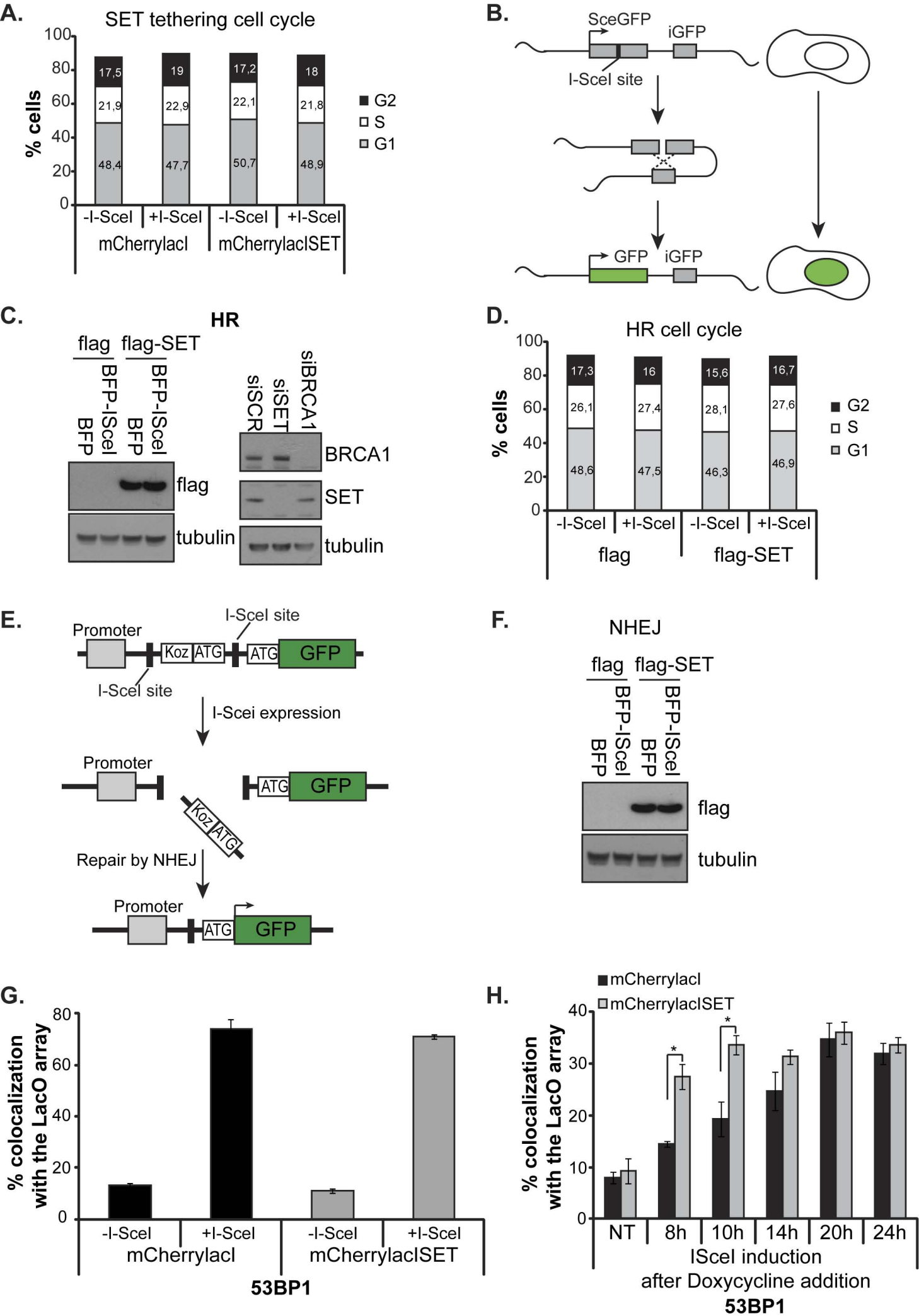

Figure S5 (Related to Figure 5)

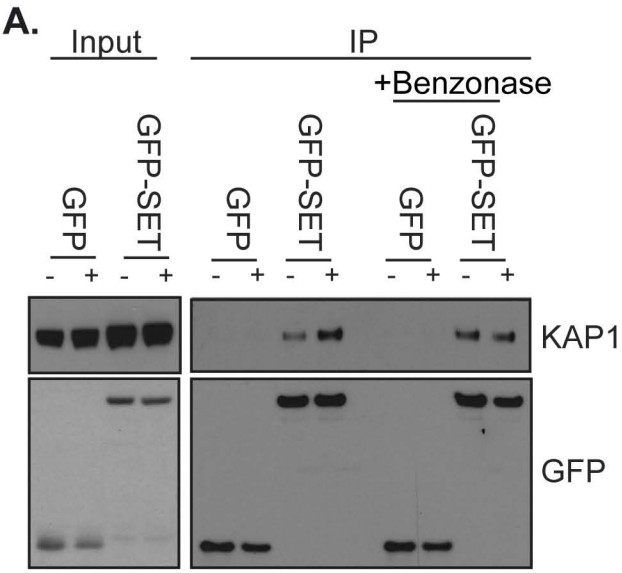

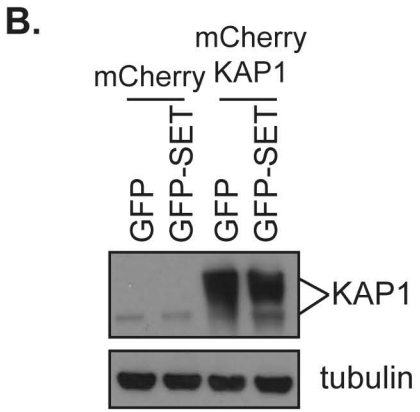

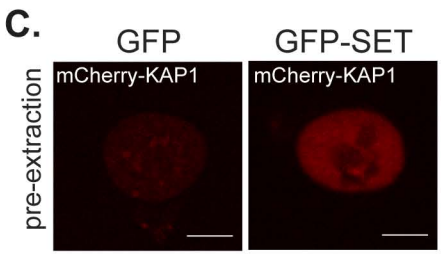

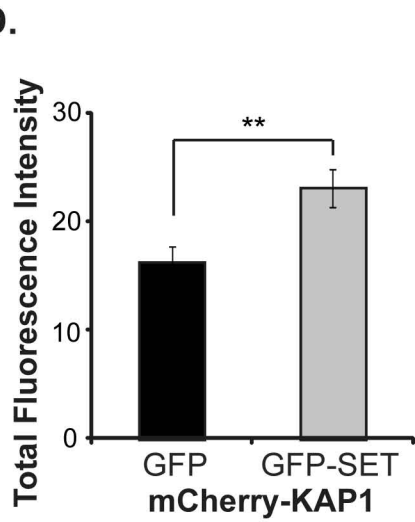

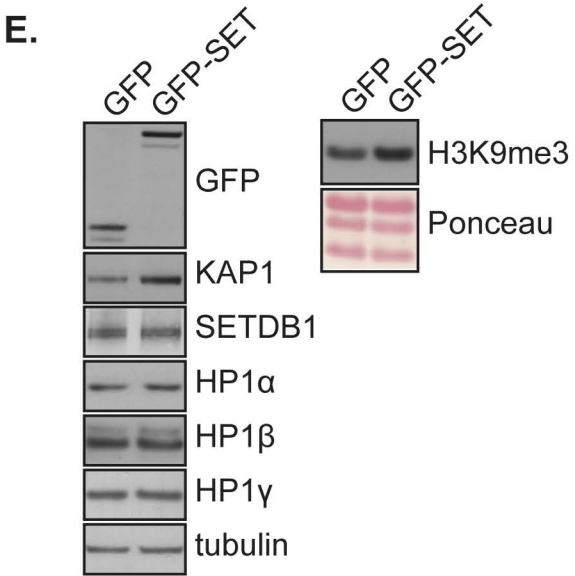

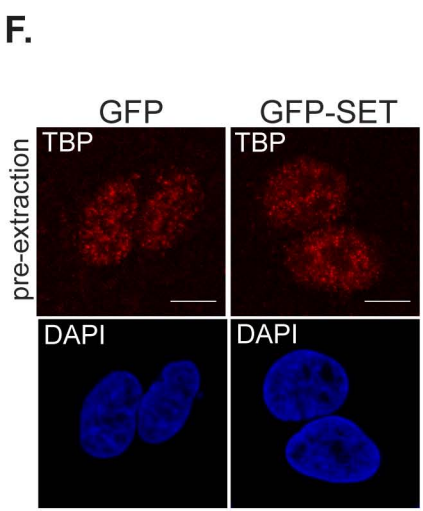

Figure S6 (Related to Figure 6)

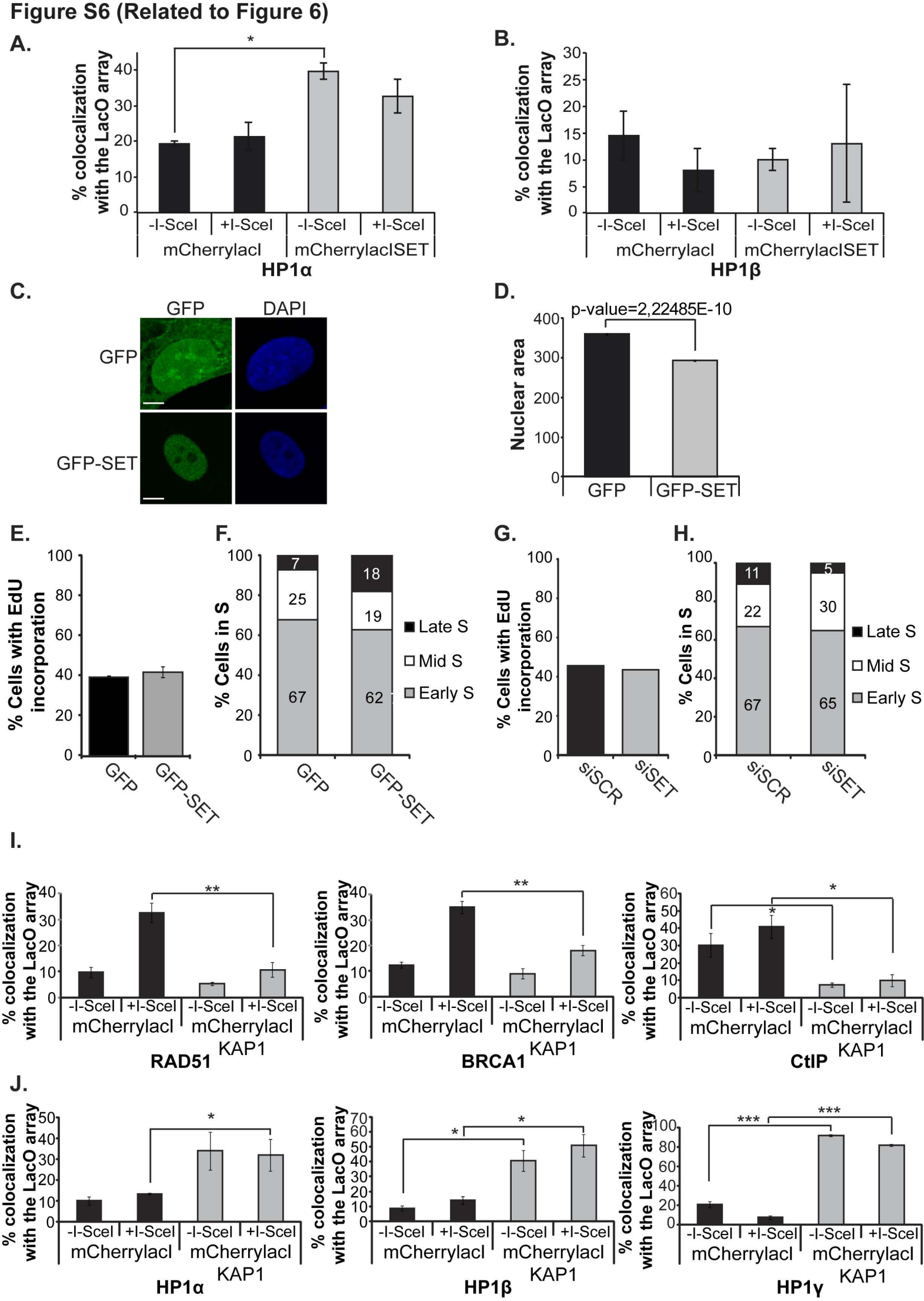

Figure S7 (Related to Figure 7)

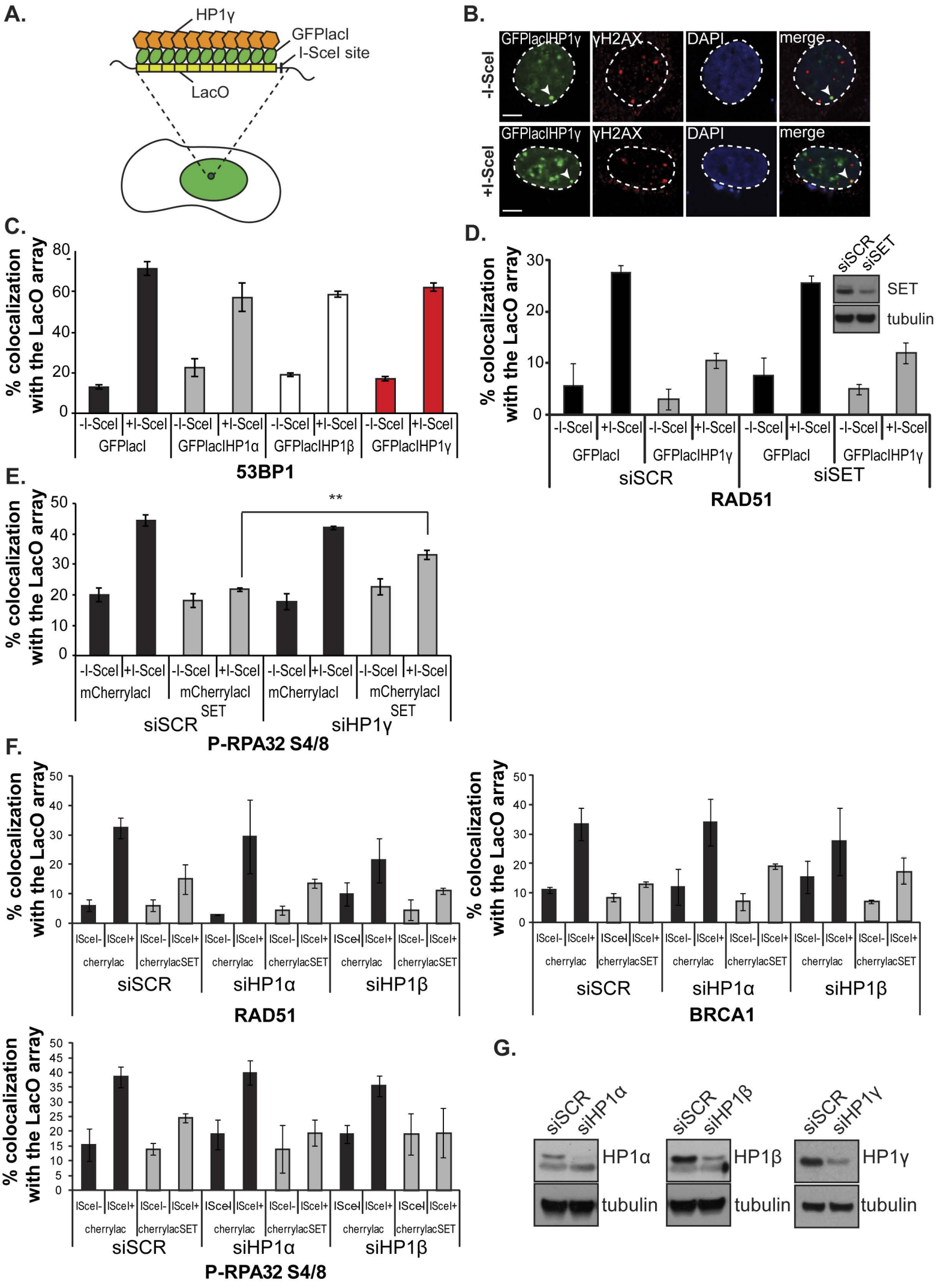

Supplemental Figure Legends

Figure S1 (Related to Figure 1): (A) & (B) Silencing of SET as measured by relative mRNA levels or by Western blot analysis. (C) Neutral Comet assay. Left panel: U2OS cells transfected with siSCR, siSET or with siXRCC4 were treated with 200 ng/mL NCS for 15 min and released for 0 or 16h before being subjected to comet assay. Right panel: Silencing of SET and XRCC4 as confirmed by Western blot analysis. (D) Cell cycle analysis of U2OS cells transfected with siSCR (left panel) or siSET (right panel) cell lines after treatment with 50 ug/ml for 1 hour and release for the indicated time points and analyzed using Propidium Iodide staining. (E) Schematic representation of the HeLa-111-ptight cells. An array of 256 repeats of the LacO sequence flanked by an I-SceI site is stably integrated in a HeLa cell line. Upon Doxycycline addition the I-SceI enzyme is expressed and induces a double strand break at the specific I-SceI site. A set of primers targeting the adjacent Ampicilin gene is used to detect the recruitment of factors after ChIP. (F) Cell cycle analysis of HeLa-111-ptight cells treated with Mimosine or RO3306 and analyzed using Propidium Iodide staining to verify G1-S and G2 arrest respectively. See also Figure 1.

Figure S2 (Related to Figure 2): (A) Schematic representation of the fusion proteins stably overexpressed in U2OS cells (GFP and GFP-SET) (B) upper panel: U2OS stable cell lines expressing either GFP or GFP-SET. Lower panel: Immunofluorescence of endogenous SET in U2OS cells (scale bar: 10 µm). (C) Total cell extracts from U2OS GFP and GFP-SET cells were analyzed by Western blot against the proteins GFP, SET and tubulin. (D) Biochemical fractionation of U2OS-GFP and U2OS-GFP-SET cells. All fractions were analyzed by Western blot. (E) Clonogenic survival of U2OS cells stably overexpressing GFP or GFP-SET with increasing concentrations of Phleomycin. SEM represents the errors from 3 independent experiments. Statistical significance was calculated using the t-test (P<0,05 *, P<0,01 **, P<0,001 ***). (F) Cell cycle analysis of U2OS-GFP (left panel) and U2OS-GFP-SET (right panel) cell lines after treatment with 50 µg/ml Phleomycin for 1 h and release for the indicated time points using Propidium Iodide staining. (G) BrdU cell cycle analysis of U2OS-GFP and U2OS-GFP-SET cells after treatment with 2 mM Hydroxyurea (HU) for 24 hrs

and release for the indicated time points. (H) Duplication time of U2OS-GFP and U2OS-GFP-SET cells. 10^5 cells from each cell line were grown for 24h, 48h and 72h and the total number of cells was measured at the indicated time points. See also Figure 2.

Figure S3 (Related to Figure 3): (A) Left panel: Immunofluorescence staining of U2OS GFP and GFP-SET cells with γH2AX after treatment with 10 mM HU for 24h and release for another 8 h (scale bar: 10 μm). Right panel: Quantification of γH2AX positive cells after treatment with 10 mM HU and release for the indicated time points. Photos of at least 100 cells were analyzed for each condition. SEM represents the errors from 3 independent experiments. (B) Cell cycle analysis of GFPlacI-lacO U2OS cells transfected with flag, flag-SET using Propidium Iodide staining. (C)&(D) Quantification of RAD51 foci positive cells (>3 foci per cell) or BRCA1 foci positive cells (>5 foci per cell) after treatment with 50 ng/ml NCS and release for the indicated time points. SEM represents the errors from 3 independent experiments. Statistical significance was calculated using the t-test (P<0,05 *, P<0,01 **, P<0,001 ***). (E) Cell cycle analysis of U2OS-GFP (left panel) and U2OS-GFP-SET (right panel) cell lines after treatment with 50 ng/ml NCS for 15 min and release for the indicated time points using Propidium Iodide staining. See also Figure 3.

Figure S4 (Related to Figure 4): (A) Cell cycle analysis of lacO U2OS cells transfected with flag, flag-SET or mCherrylacI, mCherrylacISET using Propidium Iodide staining. (B) Schematic representation of the DR-GFP system. The upstream (5′) GFP gene (cassette I) carries a recognition site for I-SceI, a rare-cutting endonuclease that does not cleave several eukaryotic genomes tested. The downstream (3′) GFP (cassette II) is inactivated by upstream and downstream truncations, leaving only ~502 bp of GFP. Expression of the meganuclease I-SceI leads to formation of DSBs and GFP reconstitution is a marker of HR efficiency. (C) Overexpression of SET (left panel) or silencing of SET and BRCA1 (right panel) in DR-GFP cells as confirmed by Western blot analysis. (D) Cell cycle analysis of U2OS-DR-GFP cells transfected with flag, flag-SET or siSCR, siSET, siBRCA1 using Propidium Iodide staining. (E)

Schematic representation of the NHEJ system (GCV6 cells). The GCV6 cell line used contains a GFP-based NHEJ reporter substrate in which the I-SceI cleavage sites are separated by a Kozak ATG cassette which prevents the expression due to a wrong ORF. Upon expression of I-SceI the Kozak ATG sequence is cut off the DSBs are repaired by NHEJ and there is expression of GFP. (F) Overexpression of SET in GCV6 cells as confirmed by Western blot analysis. (G) Quantification of the co-localization of 53BP1 foci with the lacO array in at least 100 lacO U2OS cells transfected with mCherrylacI or mCherrylacISET in the presence or absence of transiently overexpressed I-SceI (16 hour transient transfection). SEM represents the errors from 3 independent experiments. (H) Quantification of the co-localization of 53BP1 foci with the lacO array in at least 100 lacO U2OS cells transfected with mCherrylacI or mCherrylacISET during a time course of I-SceI inducible expression upon Doxycycline addition. SEM represents the errors from 3 independent experiments. Statistical significance was calculated using the t-test (P<0,05 *, P<0,01 **, P<0,001 ***). See also Figure 4.

Figure S5 (Related to Figure 5): (A) Immunoprecipitation (IP) of cell extracts from U2OS GFP and GFP-SET cells treated or not with 10 mM of HU in the presence or absence of Benzonase using the GFP-trap column. The inputs and eluates were analyzed by Western blot against the proteins KAP1 and GFP. (B) U2OS-GFP and U2OS-GFP-SET cells were transfected with mCherry or mCherry-KAP1 and the extracts were analyzed by Western Blot. (C) U2OS-GFP and U2OS-GFP-SET cells were transfected with mCherry or mCherry-KAP1 and fixed after pre-extraction of soluble proteins (scale bar: 10 μm). (D) Levels of mCherry intensity were measured by an automated microscope. (E) Western blot analysis of whole cell extracts (left panel) or histone extracts (right panel) of U2OS-GFP and U2OS-GFP-SET cells against GFP, KAP1, SETDB1, HP1α, β and γ, tubulin and H3K9me3. Ponceau staining was used to show equal loading on histone extracts. (F) Immunofluorescence staining of U2OS-GFP and U2OS-GFP-SET cells for TBP protein after pre-extraction of soluble proteins (scale bar: 10 μm). See also Figure 5.

Figure S6 (Related to Figure 6): (A)&(B) Quantification of the colocalization of HP1α and HP1β foci with the LacO array in at least 100 lacO U2OS cells transfected with mCherryLacI or mCherryLacISET in the presence or absence of I-SceI. SEM represents the errors from 3 independent experiments. Statistical significance was calculated using the t-test (P<0,05 *, P<0,01 **, P<0,001 ***) (C) U2OS cells expressing either GFP or GFP-SET (scale bar: 10 μm). (D) Quantification of the nuclear area as defined by DAPI staining. (E) Quantification of positive cells for EdU incorporation amongst U2OS-GFP and U2OS-GFP-SET cells. (F) Quantification of EdU positive cells in early, mid or late S phase according to their staining pattern in U2OS-GFP and U2OS-GFP-SET cells. (G) Quantification of positive cells for EdU incorporation in U2OS cells transfected with siSCR or siSET. (H) Quantification of EdU positive cells in early, mid or late S phase according to their staining pattern in U2OS cells transfected with siSCR or siSET. (I)&(J) Quantification of the co-localization of RAD51, BRCA1, CtIP, HP1α, HP1β or HP1γ foci with the LacO array in at least 100 lacO U2OS cells transfected with mCherrylacI or mCherrylacIKAP1 in the presence or absence of I-SceI. SEM represents the errors from 3 independent experiments. Statistical significance was calculated using the t-test (P<0,05 *, P<0,01 **, P<0,001 ***). See also Figure 6.

Figure S7 (Related to Figure 7): (A) Schematic representation of HP1γ tethering on the lacO-lacI/I-SceI system. (B) Immunofluorescence staining of the lacO U2OS cells transfected with GFPlacIHP1γ with γH2AX antibody in the presence or absence of I-SceI showing the colocalization of γH2AX foci with the lacO array in the presence of I-SceI (scale bar: 10 μm). (C) Quantification of the colocalization of 53BP1 foci with the lacO array in at least 100 lacO U2OS cells transfected with GFPlacI or GFPlacIHP1α, GFPlacIHP1β or GFPlacIHP1γ in the presence or absence of I-SceI. (D) Quantification of the colocalization of RAD51 foci with the lacO array in at least 100 lacO U2OS cells transfected with siSCR or siSET, followed by transfection with GFPlacI or GFPlacIHP1γ in the presence or absence of I-SceI. Silencing of SET was verified by Western blot. (E) Quantification of the colocalization of P-RPA32 S4/8 foci with the lacO array in at least 100 lacO U2OS cells transfected with siSCR or siHP1γ, followed by transfection with mCherrylacI or mCherrylacISET in the

presence or absence of I-SceI. (F) Quantification of the colocalization of RAD51, BRCA1 and P-RPA32 S4/8 foci with the lacO array in at least 100 lacO U2OS cells transfected with siSCR or siHP1α or siHP1β, followed by transfection with mCherrylacI or mCherrylacISET in the presence or absence of I-SceI. (G) Silencing of HP1α, β and γ as confirmed by Western blot analysis. See also Figure 7.

Supplemental Experimental Procedures

siRNA screen

Screening was performed at the high throughput screening facility of the IGBMC, using a custom siRNA library (Dharmacon) of chromatin related and phosphatome siRNA smartpool (4 different siRNAs/pool). Controls were performed with smartpool siRNAs from Dharmacon (Thermo Scientific): siRNAs against human XRCC4 (positive control) and siGFP (negative control). For each target, 25 nM final concentration of siRNA is reverse transfected in 5,000 HeLa cells per 0.3 cm^2 by using Interferin (Polyplus). All screens were performed in 96-well cell culture microplates with a particular focus on avoiding microplate edge effects. γH2AX and 53BP1 foci were analyzed by immunofluorescence 3 days after siRNA transfection and 16 hrs after NCS treatment (100 ng/mL, 15 min). Cells were washed, fixed with 3% paraformaldehyde, permeabilized with 0.1% Triton X-100, blocked with 2% BSA, and incubated with γH2AX and 53BP1 antibodies followed by Alexa Fluor 488 and 568 conjugated second antibodies (Invitrogen). Cell nuclei are counterstained with 1 µg/mL DAPI. The screens were achieved owing to a TECAN robotic station (for cell transfection, staining, and immunocytochemistry) and to a Caliper Twister II robotic arm coupling microplate stacks to the InCELL1000 analyzer microscope (GE LifeSciences). Images were acquired with the InCELL1000 analyzer microscope (GE LifeSciences) and analyzed with the Multi Target Analyzer from GE Healthcare (γH2AX intensity and 53BP1 foci counting). Datasets were analyzed via RReportGenerator software (Wolfgang Rafelsberger, IGBMC).

Laser microirradiation

For 405 nm UV-laser irradiation, experiments were carried out as described by Kruhlak et al., (2006). Briefly, cells pre-treated with 2 uM Hoechst 33342 (Sigma-Aldrich) for 5 min were imaged at 37°C using a custom built Zeiss Cell Observer Microscope (Intelligent Imaging Innovations (3i), Boulder, Co), equipped with a heated CO_2 incubator, diode-based lasers (405, 488, 561, and 633 nm) and a spinning-disk confocal scanning unit X1 (CSU-X1)(Yokagawa, Japan) using a 40× (1.4 NA)

immersion oil objective lens. UV-laser damage was induced by a 100 mW 405 nM diode laser using a Vector Scan Unit (3i), where the effective light output was measured as ~8 mW at the objective when using 100% power. A single line scan of the 405 nm laser at 70% power was sufficient to generate DNA DSBs as demonstrated by the rapid recruitment of KU80, which was estimated to be equivalent to ~40-60 Gy cellular dose by the method above. Images were captured every 10 s for 6 min, and analyzed using an Evolve EMCCD camera (Photometrics) and Slidebook 5.5 software (3i), respectively. A minimum of 25 cells were irradiated and tracked over time per condition.

Immunofluorescence

Cells were grown on glass coverslips, fixed in 4% paraformaldehyde in PBS for 10 min at room temperature and permeabilized with 0.5 % Triton-X100 in PBS for 10 min at room temperature. Following permeabilization cells were blocked with 1 % BSA in PBS-Tween 0.1%(PBST) for 1 hr at room temperature. Blocked cells are then stained with the appropriate primary antibody diluted in 1 % BSA in PBST for 1 hr at room temperature. Cells were then washed with PBST and stained with a fluorescent secondary antibody (Alexa Fluor, Molecular Probes) for 45 min at room temperature. Finally, the cells were washed with PBST and the coverslips were mounted using Vectashield with DAPI (Vector Laboratories Inc). In case of pre-extraction of soluble proteins, the cells are incubated with Pre-extraction buffer (0.5 % triton-100, 50 mM Hepes pH 7, 150 mM NaCl, 10 mM EGTA, 2mM MgCl2) for 30 sec on ice prior to fixation. Antibodies used are: mouse anti γH2AX and H3K9me3 (Abcam), rabbit anti RAD51 PC130 (Calbiochem), rabbit anti-BRCA1 sc642 (Santa Cruz), mouse anti-CtIP clone 14-1 (Active Motif), rabbit anti-P-RPA 32 S4/8 and rabbit anti-53BP1 (Bethyl Laboratories), mouse anti KAP1, mouse anti-HP1α, mouse anti-HP1β and mouse anti-HP1γ (Euromedex). In the case of EdU incorporation experiments the Click-iT® EdU Alexa Fluor® 488 Imaging Kit was used according to the manufacturer's protocol.

Tissues from head and neck cancer were deparaffinized and rehydrated. Blocking was performed with 1% BSA and 1/20 normal goat serum in TBS. Following, heat

induced antigen retrieval was carried out in citrate buffer pH: 6.00 for 20 min. The antibodies used were rabbit anti-H3K9me3 (1/200, Abcam), rabbit SET (1/50, Santa Cruz) and mouse HP1γ (1/200). Tissues were incubated with anti-mouse and anti-rabbit fluorescent secondary antibodies and DAPI.

Western blot

U2OS cells were harvested in RIPA buffer (25 mM Tris-HCl pH 7.6, 150 mM NaCl, 1% NP-40, 0.5% sodium deoxycholate, 0.1% SDS) supplemented with protease inhibitor cocktail (Roche) and incubated for 15 min on ice before centrifugation (15 min, 14 000 rpm, 4 °C). The quantity of protein was determined by Bradford (Bio-Rad). The extracts were analyzed by SDS-PAGE. Primary detection antibodies are diluted in 1% non-fat dry milk in PBS. Antibodies used are rabbit anti-SET/I2PP2A (santa cruz) or rabbit anti-SET/I2PP2A (Globozymes), mouse anti-phospho-Histone H2AX (Ser139) clone JBW301 (Merck Millipore), rabbit anti-H2AX and goat anti-GFP (abcam), , rabbit anti-PChk1, rabbit anti-PChk2, rabbit anti-Chk1 (Cell Signaling), mouse anti-Chk2 (Upstate), mouse anti-alpha-tubulin T9026 (Sigma) and anti-XRCC4 (santa cruz).

Chromatin Immunoprecipitation (ChIP)

The ChIP was performed as previously (Lemaitre et al., 2014). Briefly, two 150-mm dishes with HeLa-111-ptight cells that were 70% confluent were used for each time point. The cells were crosslinked for 30 min in 0.75% (v/v) paraformaldehyde and then sonicated in 1% (v/v) SDS-containing sonication buffer (50 mM HEPES, pH 8, 140 mM NaCl, 1 mM EDTA, 1% (v/v) TritonX-100, 1% (v/v) SDS and a protease inhibitor cocktail (Roche)). Thirty milligrams of chromatin were diluted in RIPA buffer (50 mM Tris-HCl, pH 8, 150 mM NaCl, 1 mM EDTA, 1% Triton X-100 (v/v), 0.1% sodium deoxycholate (w/v) and 0.1% SDS (v/v)) and were used in each immunoprecipitation by adding 4 µg of antibody and 50 µl of protein-A and protein-G sepharose beads (Sigma). The beads were washed for 5 min with low-salt buffer (20 mM Tris-HCl, pH 8, 150 mM NaCl, 2 mM EDTA, 1% (v/v) Triton X-100 and 0.1% (v/v) SDS), then 5 min with high-salt buffer (20 mM Tris-HCl, pH 8, 500 mM NaCl, 2

mM EDTA, 1% (v/v) Triton X-100 and 0.1% (v/v) SDS) and for 5 min with LiCl buffer (10 mM Tris-HCl, pH 8, 250 mM LiCl, 1 mM EDTA, 1% (v/v) NP-40 and 1% (w/v) sodium deoxycholate) and two times for 5 min with TE buffer. The elution was done twice at 65 °C for 15 min. Cross-links were reversed by incubation at 65 °C for 6 h. The DNA was purified after proteinase K and RNaseA treatment by using phenol-chloroform extraction and was resuspended in 50 µl of TE buffer. The signal in each experiment was calculated using the formula (immunoprecipitated sample–IgG control)/input, and each value represents a relative DNA concentration that is based on the standard curve of the input.

Histone extraction

Cells were harvested and washed twice with ice cold PBS. The cells were then resuspended in Triton extraction buffer (TEB) (0.5 % triton X-100, 2 mM PMSF, 0.02 % NaN3, 1X PBS) at cell density of 10^7 cell/mL and were incubated on ice for 10 min with gentle stirring before being centrifuged at 2000 rpm for 10 min at 4 °C. The pellet was then washed in half the volume of TEB, centrifuged and resuspended in 0.2 N HCl at a cell density of $4x10^7$ cell/mL and incubated overnight at 4 °C. Finally the supernatant was collected, the protein quantity was determined using Bradford (Bio-Rad) and the samples were analyzed by western blot.

Cell cycle analysis

U2OS cells were treated either with phleomycin (1 h 50 µg/mL) or hydroxyurea (24h 10 mM) and released in fresh medium for the indicated time points. For cell cycle arrest experiments Mimosine (0,5 mM for 24h) was used for arrest of cells in G1-S and RO3306 (10 uM for 24h) for arrest in G2. The cells were collected using trypsin and fixed in ice-cold 70 % ethanol. The following day the cells were incubated in Propidium Iodide buffer for 30 min just before FACS analysis. For BrdU staing: BrdU (10 µM) (Sigma) was added 10 min before cell collection. Fixed cells were incubated in pepsine buffer (0.5 mg/mL pepsine, 30 mM HCl) for 10min at 37°C and in HCl 2N for 20 min at room temperature. Anti-BrdU antibody (Roche) was added for 45 min before the addition of the secondary antibody (Alexa Fluor, Molecular Probes) for 30

min. Finally cells are washed and incubated in Propidium Iodide buffer and analyzed by FACS. Acquisition of the data is performed through Cell Quest software, and analysis through FlowJo and ModFit.

Survival assays

U2OS cells were plated in 6 well plates in triplicates (500 cells per well) and were subsequently treated with increasing concentrations of either phleomycin (Sigma) or camptothecin (Sigma) for 1 hour. The cells were then released with the addition of fresh medium and were let to grow in colonies for 10 days. After 10 days, the cells were washed with PBS, fixed with 4% Formaldehyde for 30 minutes and stained with Crystal Violet (0,1% w/v) for 1 hrr. The number of colonies per well was measured by ImageJ.

Comet assay

Neutral Comet assay was performed according to the manufacturer's protocol (Trevigen Kit for Comet assay). Briefly, U2OS cells were treated with NCS (200 ng/ml) for 15 minutes and were collected either immediately or 16 hours after the treatment. 5000 cells from each condition were combined with Low Melting Agarose (LMAgarose) at a ratio of 1:5 and were placed onto a CometSlide. The slides were treated according to the Trevigen kit protocol and were finally electrophorized for 15 min at 21 V at 4^{o}C. The slides were subsequently stained with SYBR green and photos were acquired using a Leica epifluorescence microscope DM600B. Photos of at least 100 cells were analyzed by CometScore and the average Comet Tail Moment was measured.

RNA extraction and RT-qPCR

RNA was extracted from cells using the RNeasy kit (Qiagen) according to the manufacturer instructions. RT-qPCR was then performed with the Quantitect SYBR Green RT-PCR Kit (Qiagen) in the LightCycler 480 system (Roche).

Human samples

Formalin-fixed, paraffin-embedded specimens from 10 surgically removed colon carcinomas and 15 head and neck carcinomas were analyzed, after local ethical committee approval. In addition, adjacent normal tissue was included from each specimen examined. Patients had not undergone any chemo-, radio- or immunotherapy prior to surgical resection, to avoid any influence in the expression status of the examined factors. The majority of the samples have been described in previous reports (Liontos et al., 2007; Evangelou et al., 2013).

Immunohistochemistry (IHC)

Method: An immunoperoxidase staining was performed on serial sections of the tissues using the UltraVision LP Detection System kit from Thermo Scientific. Heat induced antigen retrieval was carried out in citrate buffer pH: 6.00 for 25 min. The antibodies used were anti-H3K9me3 (1/1.500+1/40 goat serum, Abcam), SET (1/500, Santa Cruz) and HP1γ (1/600, Millipore). For color development we used 3,39-diaminobenzidine tetrahydrochloride (DAB) and hematoxylin as counterstain. For tissue sections observation and image capturing a Leica microscope was employed.

Evaluation: Only nuclear staining was taken into consideration. The IHC staining was evaluated under optical microscope in 5 high-power fields (X400) per slide. The selected fields were identical in all serial sections to enable optimal comparison. The evaluation was done by 2 independent qualified pathologists.

Controls: Colon carcinoma sections were used as positive controls as suggested by the antibody manufacturer. As negative controls tissue sections stained by omitting application of the primary antibody were used.